University of California
Los Angeles

Spatio-temporal Excitation-emission Multiplexing for Multifocal 2-photon Calcium Imaging in Deep Tissue

A dissertation submitted in partial satisfaction of the requirements for the degree Doctor of Philosophy in Physics

by
Adrian Cheng

2010

Copy Page

This page intentionally left blank

The dissertation of Adrian Cheng is approved.

X

Dolores Bozovic
Professor

X

Carlos Portera-Cailliau
Professor

X

Robijn Bruinsma
Professor

X

Katsushi Arisaka
Professor, Committee Chair

University of California, Los Angeles

2010

Table of Contents

List of Figures

List of Tables

VITA

April 25, 1984	Born, San Francisco, California
2004-2005	Junior Engineer Institute for Geophysics and Planetary Physics at UCLA
2006	B. S. Phyics B. S. Pure Mathematics M. S. Physics University of California, Los Angeles
2007	Junior Development Engineer Department of Physics and Astronomy University of California, Los Angeles
2008	Teaching Assistant Department of Physics and Astronomy University of California, Los Angeles
2007-	Graduate Student Researcher Department of Physics and Astronomy University of California, Los Angeles
2009-	Graduate Student Researcher Neural Microcircuits Training Program David Geffen School of Medicine University of California, Los Angeles

PUBLICATIONS AND PRESENTATIONS

A. Cheng, J. Tiago Gonçalves , P. Golshani , K. Arisaka, C. Portera-Cailliau. Spatio-temporal excitation-emission multiplexing for multifocal 2-photon calcium imaging in deep tissue. Society for Neuroscience, 2009

R. Colyer, G. Scalia, F. Guerrieri, A. Cheng, M. Levi, D. Aharoni, K. Arisaka, J. Millaud, M. Ghioni, S. Tisa, F. Zappa, S. Cova, S. Weiss, X. Michalet. High throughput single-molecule spectroscopy with highly parallel excitation and detection. Biophysical Society Meeting 2010.

A. Cheng, C. Morgado, L. Beltra-Parrazal, et al. An intensified CMOS imager for sub-millisecond
fluorescence microscopy. Society for Neuroscience 2008.

X. Michalet, A. Cheng, J. Antelman, M. Suyama, K. Arisaka, S.
Weiss. Hybrid photodetector for single-molecule spectroscopy and microscopy. Proceedings of SPIE.
2008;6862(1):68620F-68620F-12.

L. Fredrickson, A. Cheng, C. E. Strimbu, D. Bozovic, and K. Arisaka. The use of a CMOS camera
to resolve nanometer displacements of hair cell stereocillia in the bullfrog sacculus. Proceedings of
SPIE. 2008;6859(1):68591B-68591B-7.

A. Cheng, A. Calvez, T. Ohnuki, A. Tripathi, J. Lee, K. Arisaka. Preliminary Search for Thread-like Multiplet Anisotropy in Auger Data. Pierre-Auger GAP Note 2006.
M. Ashour-Abdalla, J. Bosqued, M. El-Alaoui, V. Peroomian, R. Walker, L. Zelenyi, J. Wright, A. Cheng. Multiscale plasma structuring near the boundary of open-closed field lines. American Geophysical Union, Fall Meeting 2004, #SM13C-06.

ABSTRACT OF THE DISSERTATION

Spatio-temporal Excitation-emission

Multiplexing for Multifocal 2-photon Calcium Imaging

in Deep Tissue

by

Adrian Cheng

Doctor of Philosophy in Physics

University of California, 2010

Professor Katsushi Arisaka, Chair

Calcium imaging using 2-photon laser scanning microscopy is an ideal tool for interrogating large ensembles of neurons in the intact brain, but suffers from poor temporal resolution when using conventional raster scanning. Using multiple laser beams can increase image acquisition rates. Unfortunately, this approach is highly sensitive to light scattering in brain tissue, which precludes the use of camera-type detectors necessary to distinguish fluorescence from different beams. To circumvent this problem, one can introduce a spatio-temporal multiplexing approach separating multiple beams in time by the fluorescence lifetime of the calcium dye. The scattered fluorescence emission from individual beams is distinguished by a state-of-the-art single-channel hybrid photomultiplier. By combining this method with fast raster scanning, millisecond acquisition rates are achieved for high-resolution in vivo calcium imaging of ~100 layer 2/3 neurons in barrel cortex. Additionally, recording of neuronal activity in multiple axial planes at rates of tens of milliseconds is achieved, by scanning individual beams at different tissue depths. This is the first time multiple plane calcium imaging has been achieved in-vivo.

Preface

On first look, it is not obvious why Physicists and Neuroscientists have any overlap in research interests or activities. In the field of biomedical physics, the relationship is clear, and the same is true in areas such as macromolecular and membrane biophysics and nerve conduction. However the relatively unassuming field of neuroimaging has seen a lot of contribution from people with Physics training, for example from people like Winfried Denk and David Tank. In fact, many of the graduates of David Tank's Bell Labs laboratory involved with developing two-photon imaging have had Physics or Mathematics training. Whether this was by necessity or by some other phenomenon maybe isn't so clear. Being able to image dense fluorescence labeled

neuronal networks must have been something intrinsically exciting to these people, as two-photon microscopy seems to be used exclusively for this purpose today.

A similar intrinsic interest was sparked when Consuelo Morgado-Valle showed us some calcium imaging data from Jack Feldman's lab in the Department of Neurobiology. After discovering the small UCLA calcium imaging community, I began to get involved in Katsushi Arisaka's activities introducing different vacuum tube photodetectors to their experiments. The work here—a continuous four-year long effort to achieve faster, more precise, and less invasive calcium imaging in neuronal networks—is based on those initial experiments, as well as on the work of Peyman Golshani and the Portera lab, which had already been carrying out large amounts of calcium imaging experiments in-vivo.

The contribution to two-photon calcium imaging presented here could be considered to be small and incremental at best. However the many small bits of test data collected along the way (not shown) seem to indicate that both the emitted and collected fluorescence in calcium imaging experiments can still be increased by the orders of magnitude needed to realize ideal millisecond calcium imaging over hundreds of neurons. I hope our work on spatio-temporal multiplexed two-photon imaging might somehow help towards this end.

Adrian Cheng
University of California, Los Angeles
2010

Acknowledgements

The work presented here involved contributions from a large number of people across many different laboratories. These people may or may not be aware of their essential role, as this project has evolved over many different phases.

Increasing throughput in diffraction limited biological experiments using new photodetectors at UCLA was the conception of Professor Katsushi Arisaka in the Department of Physics and Astronomy, through interaction with Dr. Xavier Michalet and Professor Shimon Weiss in the Department of Chemistry.

Initial work using high speed CMOS cameras for imaging measurements was done in the laboratory of Prof. Dolores Bozovic, by Lea Frederickson, Elliott Strimbu, and

others. Additional work was done by Jose Rodriquez and Lea Frederickson in the laboratory of Prof. John Miao.

We were first introduced to calcium imaging in neuroscience at UCLA by the laboratories of Prof. Julio Vergara, Prof. Andrew Charles, Prof. Jack Feldman, and Prof. Felix Schweizer. Preliminary work was carried out by Dr. Marino DiFranco, John Parker, and Gina Rinetti. Calcium imaging work with the intensified CMOS camera was carried out by Lea Frederickson, Dr. Consuelo Morgado-Valle, and Dr. Luis Beltran in the Feldman lab over the course of more than a year.

Two-photon microscopy was explored in the laboratory of Prof. Carlos Portera-Cailliau. Additionally my education here was largely due to the patience of Dr. Ricardo Mostany, Dr. Alberto Cruz-Martin and Dr. Jose Tiago Gonçalves. I thank Carlos and all the members of the Portera lab for their hospitality during my extended stay. Experiments in the Portera lab relevant to the work here were exclusively carried out by Dr. Jose Tiago Goncalves and Prof. Peyman Golshani.

Invaluable engineering, technical and material support was provided by Dr. Motohiro Suyama and Yoshihiko Kawai at Hamamatsu Photonics K.K. over the years, as well as Seiji Kimura and Takashi Onoume at Photron Inc. Discussions with and assistance from Prof. Jean-François Léger of the CNRS during his visit at the Portera lab were essential.

This work was initially supported by the UCLA Department of Physics and Astronomy and the UCLA Vice Chancellor for Research as well as grants from the NSF

and NIH. Eventually, it would be also be supported by grants from the NIH (NICHD and NINDS), and by the generous support of the Fu-Hsing and Jyu-Yuan Chen Family Foundation. Fellowship support was provided by the Department of Physics and Astronomy, and the UCLA Neural Microcircuits Training Program in the Department of Neurobiology at the David Geffen School of Medicine.

Introduction

Since Ramón y Cajal began sketching their large branching processes, neurons have been understood to be involved in highly connected and complex networks. In the neocortex, pyramidal neurons may receive thousands of inputs from neighbors. Dense networks of neurons are the basis for computation in the central nervous system. To reverse-engineer how these systems process information, a reasonable approach would be to characterize how their individual elements work in detail, and then study the repetitive or emergent organization of these elements. The first part of this program, the study of the membrane properties of individual neurons, has been very successful. To summarize simply, neurons accumulate a voltage over time in response to unitary input impulses, and fire an output impulse, an action potential (AP), above a threshold.

This characterization has been carried out with single glass electrode techniques, which are not suited for parallelization. So while tracing of the network connectivity is currently very feasible using existing microscopy techniques, techniques for also monitoring network activity in hundreds of cells with single electrode resolution are still being developed. As these techniques become more mature, it will become easier to design experiments addressing for example how data from different physical transducers are encoded in various parts of the nervous system, especially in downstream regions where the data is diffused over many cells and begins to interact with various types of intrinsic activity and data from other transducers or brain regions.

As neuronal networks generally occupy volumes of tissue rather than planes, one would like to be able to acquire data through opaque matter in three dimensions. Magnetic resonance imaging (MRI) and intrinsic optical signal (IOS) techniques for example can be used to probe deep brain tissue activity via changing blood-oxygen levels (here we will be mainly concerned with monitoring the mouse brain which is several cubic centimeters large). However the speed of these signals do not allow the recording of individual APs—at the scale of milliseconds—nor do they allow the recording of individual neurons—tens of microns each.

Optical imaging and microscopy techniques are particularly promising because data from many points in the object plane are acquired in parallel with diffraction-limited spatial resolution (IOS is an exception due to the diffuse nature of the contrast signal). The absorption spectrum of brain tissue also shows a window in the visible

wavelengths, between phototoxic ultraviolet and water heating near-infrared. For optical techniques, the largest problems are: accomplishing imaging through highly scattering brain tissue; generating a contrast signal in response to neural activity; and putting these two together with millisecond data collection. The first problem was solved in 1991 by Winfried Denk in the lab of Watt Webb at Cornell with the invention of 2-photon laser scanning microscopy (2PLSM) and the development of compatible in-vivo cortical imaging (Svoboda)[1-2]. The second problem has diminished with the availability of fluorescent calcium ion indicators, voltage-sensitive dyes (VSDs) and genetically encoded calcium indicators (GECIs), due to Roger Tsien, Leslie Loew and others[3-6]. Finally, the group led by Fritjof Helmchen has for example used fast laser scanning acousto-optic deflectors (AODs) to solve the last problem for a limited number of cells in a single plane[7]. Presented here is a new method for applying these fast scanning methods to 3-dimensional volumes of tissue as well as parallelizing them in general. This is achieved by spatio-temporally multiplexed laser scanning. Combined, these techniques come closer than ever to solving the problem of probing activity in large intact neuronal networks with millisecond-micron resolution.

Epifluorescence Calcium Imaging

As a complement to optical microscopy techniques based on intensity or phase differences of transmitted or scattered light, fluorescence microscopy has become an

important tool for studying biological tissues with diffraction-limited resolution. Fluorescence microscopy—essentially imaging spectroscopy of organic compounds—allows a much higher degree of specificity, as relatively few molecules exhibit fluorescence. In many cases, local background can be reduced to zero, and in combination with single photon sensitive detectors, single molecules can be detected. Contrast specificity in a second sense can be achieved by selective expression of genetically encoded fluorescent proteins, which provides a labeling technique unavailable in other imaging modalities.

Specificity in fluorescence imaging is also demonstrated by the availability of functional fluorescence indicators. As the excitation efficiency of a fluorophore is highly dependent on its molecular characteristics, dynamic fluorescence indicators have proven useful for the detection of action potentials (APs) in individual neurons and their axons and dendrites. These indicator compounds work by combining a fluorophore molecule with a probe molecule to induce either a conformation change or change in the energies or occupation of molecular orbitals. Calcium ion indicators respond to calcium influx during APs by changing emission wavelength, intensity, lifetime, or a combination of these in the presence of calcium ions. Tuning the dissociation constant of the calcium indicator allows for a variety of dyes to span a large dynamic range. Dyes with linear response are available for nanomolar to millimolar calcium concentration changes. Additionally, using acetylmethyl-ester (AM) loading techniques, experimenters

can bathe hundreds of cells in cell-permeable emulsions of the indicator, with cell-endogenous esters rendering the compound negatively-charged and cell-impermeable.

Equipped with a fluorescence microscope, one can carry out calcium imaging experiments in a variety of thin brain slice or dissociated culture preparations. As opposed to laser scanning microscopes, epifluorescence microscopes rely on a short wavelength excitation illumination sourced by an arc lamp or light emitting diode (LED), with an emission detection camera or array separated by a dichroic mirror (figure). Neuron labeling with calcium indicator can be achieved by AM bath loading, bolus injection, or whole-cell glass electrode filling. As opposed to electrophysiology methods which per electrode can measure voltage at a single equipotential (in the cell body or on the membrane) or measure current through a single loop (through the cell to bath and ground), the fluorescence microscope and camera can record from a number of points limited mostly by camera resolution and the labeling technique. High numerical aperture microscope objectives allow diffraction-limited imaging in the two-dimensional object plane.

The resulting signals are relative increases in fluorescence brightness due to neuron APs. Influx of calcium occurs throughout the cell, and the fluorescence brightness increase is coincident with the image contour of the particular spiking cell. Dye response to calcium transients is generally very linear, and assuming so they can be characterized by an impulse response function[8]. Impulse response rise times vary across dyes, from tens of milliseconds with the Oregon Green Bapta (OGB) series to

fractions of a millisecond with low-affinity Fluo series dyes. Impulse response decay times however range from 100 milliseconds to seconds. Ultimately, signal-to-noise ratio (SNR) determines the time-resolution in a calcium imaging experiment rather than the impulse response frequency content. Assuming a single photon sensitive detector is used, emission flux per region of interest determines the relative noise level in a calcium imaging noise trace, proportional to the inverse of the square root of the photon count. This is due to the random arrival of photons at the detector over time (Poisson noise).

In an epifluorescence calcium imaging experiment, by using a powerful light source one can increase illumination flux until fluorescence saturation, photobleaching, or phototoxicity occurs. At this limit, for a certain noise limit the maximum possible acquisition rate can be achieved. To demonstrate this, we sought to perform high speed calcium imaging experiments with single AP resolution, requiring a noise level of less than one percent. Coupling an image-intensifier (II) to a high-speed camera, single photon sensitivity was achieved with a frame rate of 2000 frames per second at 512x512 image resolution. To resolve calcium transients of several percent brightness change, >10,000 photoelectrons (PEs, corresponding to detector events) are required per frame. To resolve the transients on a per pixel basis for example, this many photons are required per pixel, and many more photons are required in total. Single action potentials within bursts could be observed using calcium dyes in neurons in tissue slices (Figure 4).

These initial experiments demonstrated the possibility of increasing throughput in calcium imaging experiments to achieve millisecond-micron resolution with single AP sensitivity over many points and hence large and complicated neuronal networks. The general recipe to do so in a given optical method is to increase observation photon flux to allow the same Poisson noise over many observed points. This can be done if the effect of observation on the system remains somewhat linear and observation points remain independent. The electronic and digital capacity to handle increased data throughput is generally scalable, and the availability of high power laser sources provides a general means of focusing high light intensities on small regions.

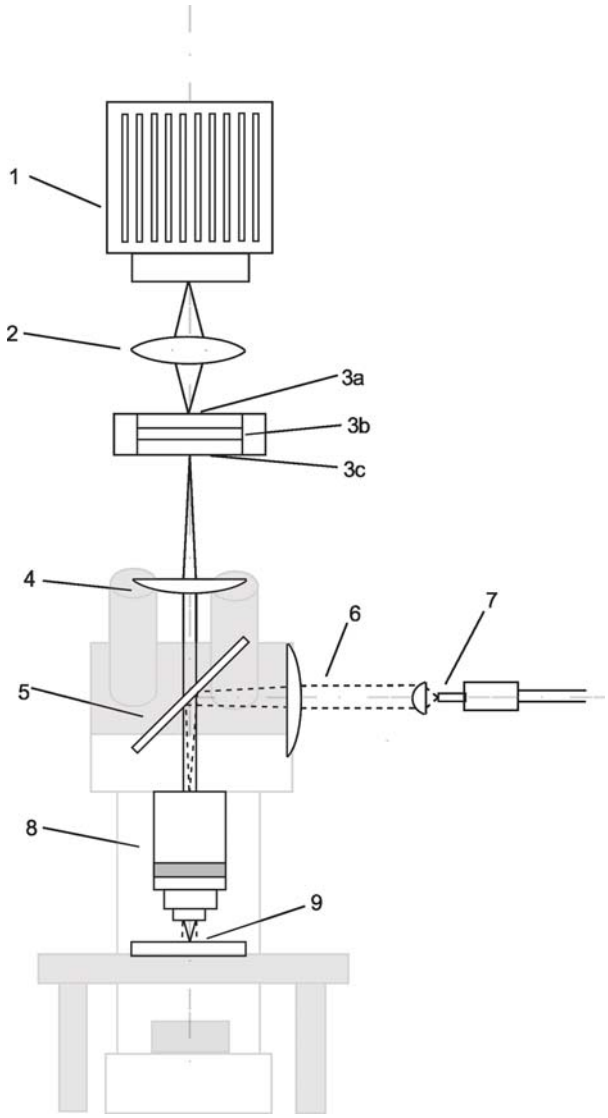

Figure 1

Experimental set-up for high-speed epifluorescence imaging

(1) High-speed camera. (2) Lens coupling. (3a) Phosphor screen. (3b) Microchannel Plate (MCP). (3c) Photocathode at tube lens image plane. (4) Tube lens. (5) Dichroic mirror. (6) Achromatic doublet pair. (7) Single-mode fiber projected onto back focal plane (BFP) of objective lens. (8) High-numerical aperture water dipping objective lens. (9) Fixed-stage for microelectrode mounting and access.

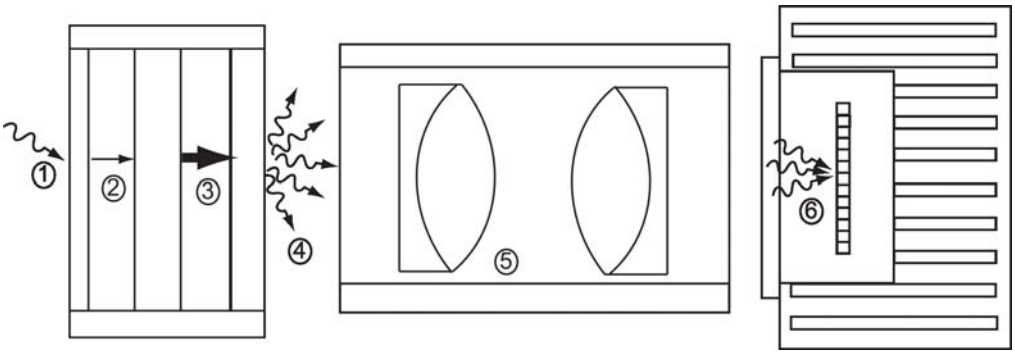

Figure 2

Intensified CMOS Imager

(1) Incoming photon strikes photocathode releasing a photoelectron, with probability equal to the quantum efficiency (QE). (2) Photoelectron in vacuum is accelerated across 200V. (3) Electrons are released after electron multiplication within a microchannel plate (MCP), with 900V and 100 gain per MCP layer. (4) Phosphorescence is emitted from phosphor screen after being accelerated across 2kV. (5) Phosphor screen is projected onto CMOS sensor inside high-speed camera (6).

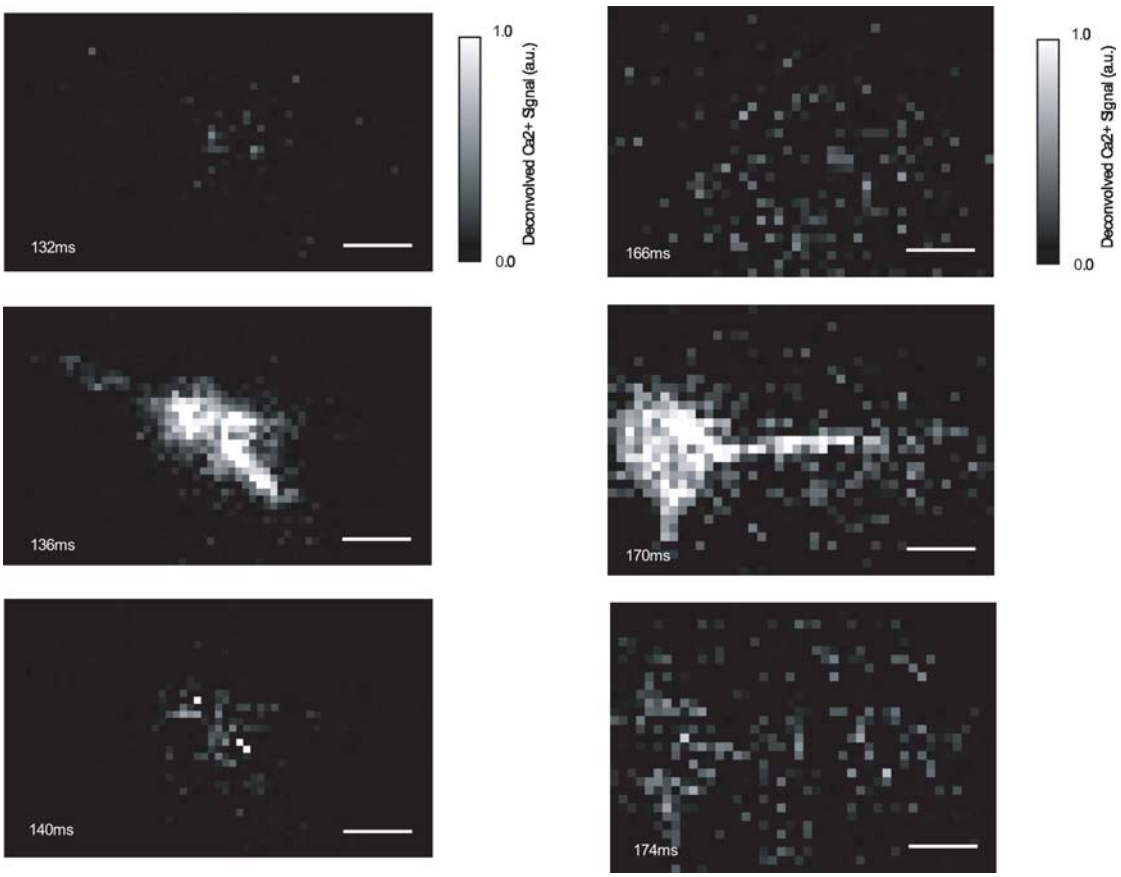

Figure 3

Calcium imaging data, deconvolved per pixel

Dendrite in experiment A (left) and soma in experiment B (right) are imaged at 1000 frames per second. Scale bar represents 10um. Time series is shown for single action potentials within bursts elicited by 300ms current injection depolarization via whole cell patch electrode. Calcium transients due to single APs are resolvable over many pixels, representing high amount of data throughput. Thus single AP sensitivity with millisecond time resolution is now extended to large sampling array.

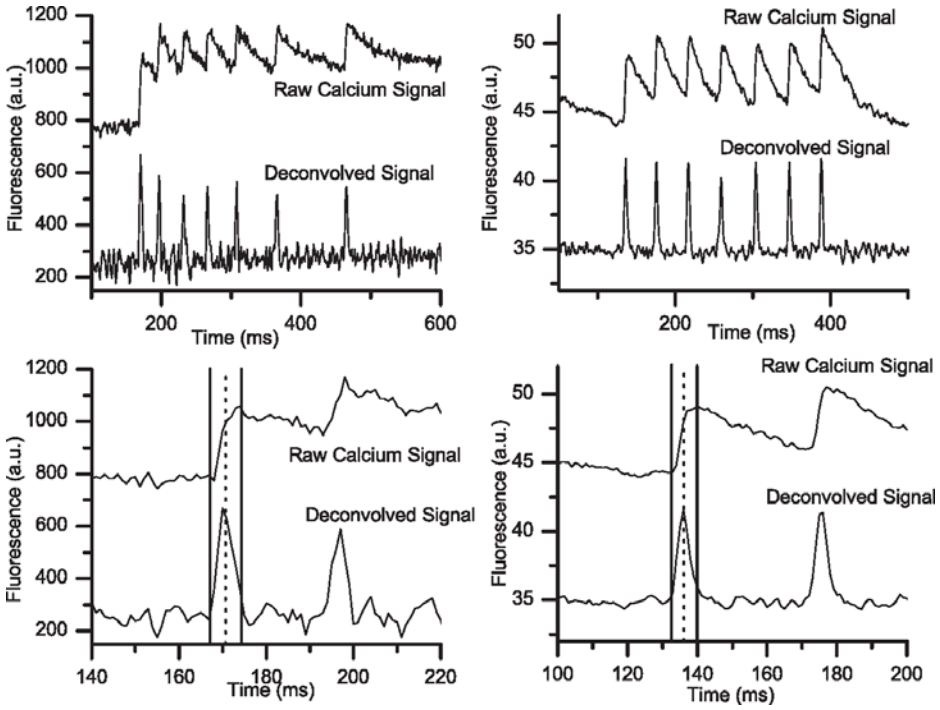

Figure 4

Raw calcium signals and deconvolved signals

(Left from top to bottom) From experiment A, raw calcium trace from region of interest, deconvolved calcium trace, and detail raw and deconvolved calcium traces. (Right) Results from experiment B. The raw calcium trace represents fluorescence emission light flux. Exponentially decaying transient impulses are present with peak relative change of approximately 20%. Deconvolution is carried out with exponential with 200ms decay. Single action potentials are easily resolvable in this case, due to high excitation light intensity.

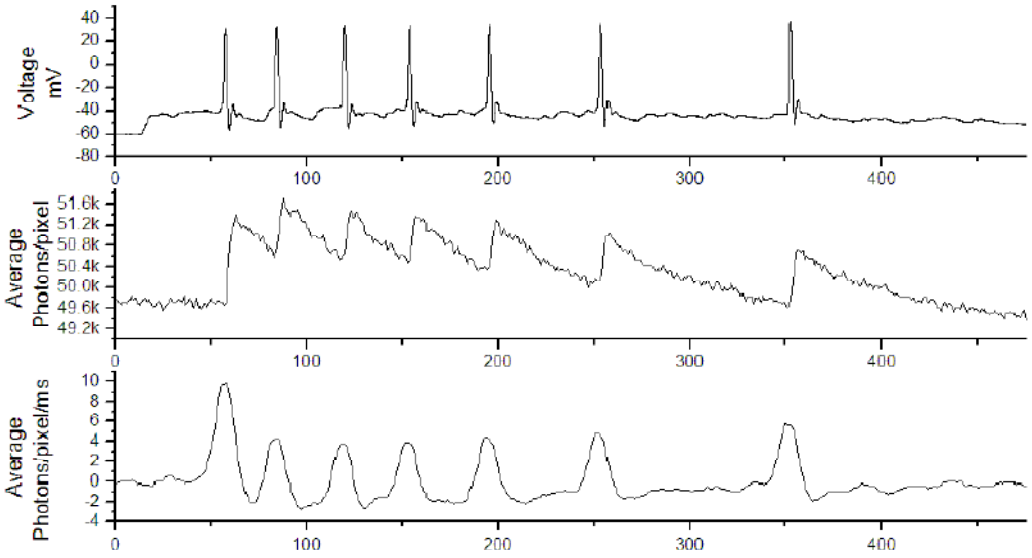

Figure 5

Simultaneous current-clamp electrophysiology trace detail for experiment A

Using a small 100 pA square current injection, a train of action potentials can be induced in cerebellar neurons. Simultaneous membrane voltage sampling verifies that each calcium transient detected during experiment A corresponds to a single action potential. Thus, calcium indicator dyes and epifluorescence microscopy allow for single action potential detection with cellular resolution.

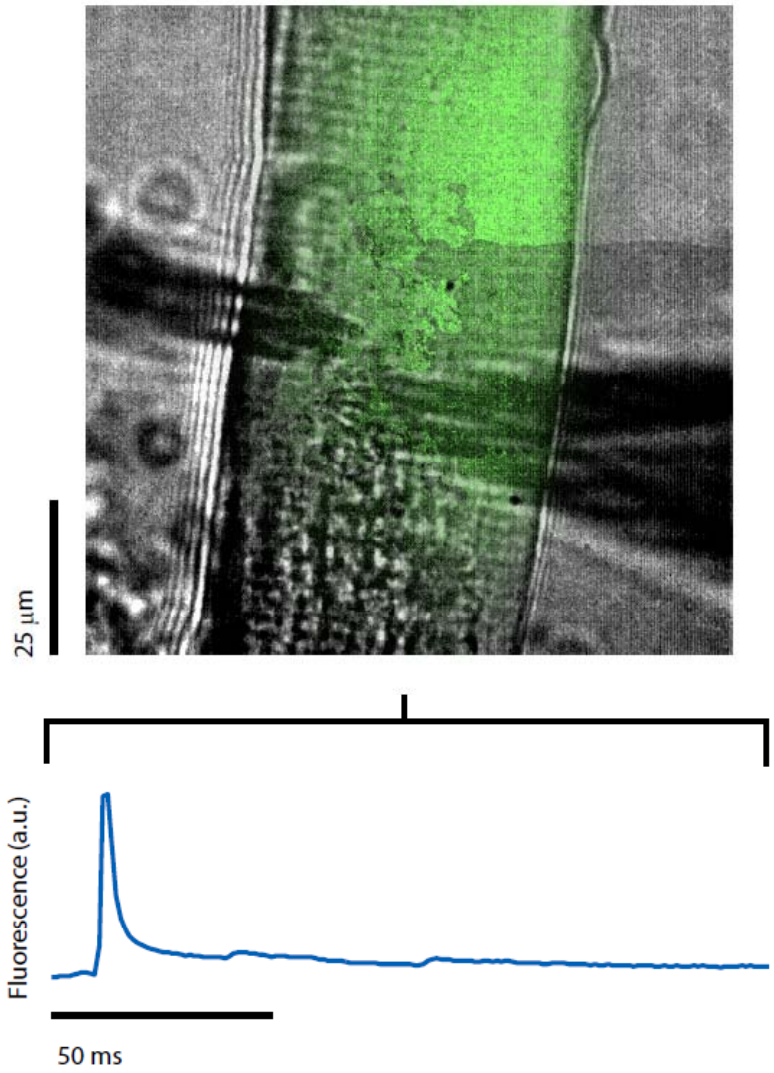

Figure 6

Voltage sensitive dye measurements in frog muscle fiber

In addition to detection of action potentials dependent calcium transients via calcium indicators, optical methods in some cases also allow direct probing of membrane potential using voltage sensitive dyes (VSDs). These dyes change fluorescence intensity in response to changing electric field strength. Shown here is a voltage transient induced in a single frog muscle fiber, and recorded by the intensified CMOS imager at 1000 frames per second.

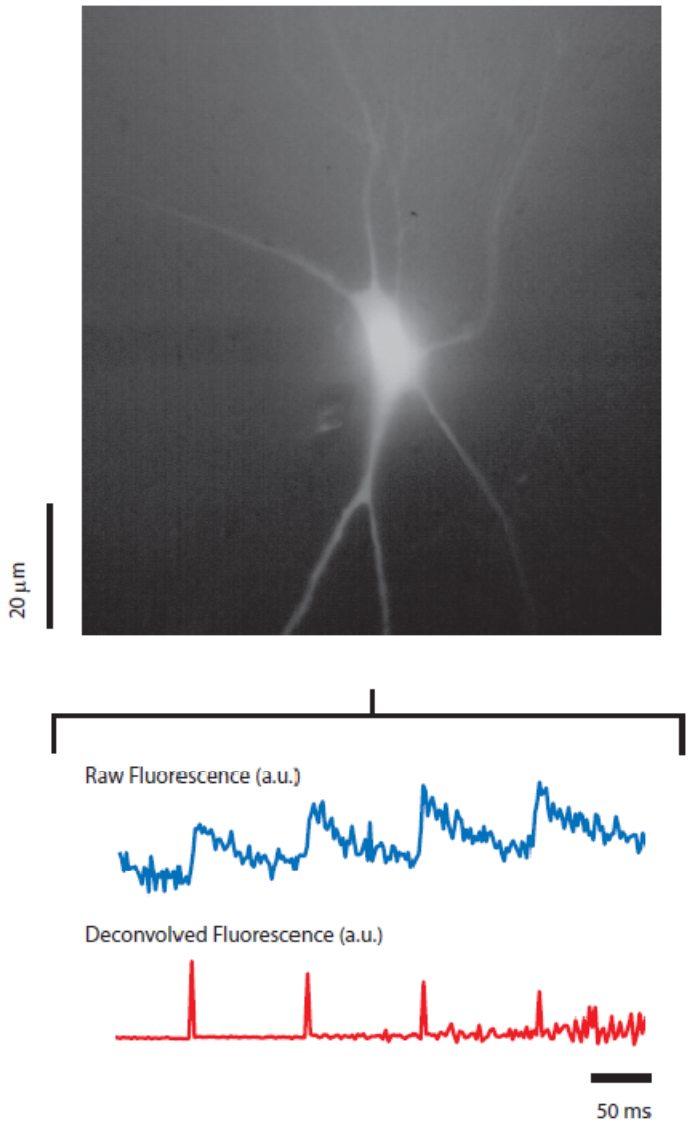

Figure 7

High speed fluorescence measurements in mouse hippocampal cultures

Imaging resolution varies across preparation types, largely due to different amounts of visible wavelength tissue scattering. Here, a single CA1 pyramidal neuron is captured using the intensified CMOS imager, with higher spatial resolution than in the previous slice preparations. In a cell monolayer, neuropil comprising of highly scattering neuronal axonal and dendritic processes is largely absent. The cell shown is labeled with the calcium indicator Fluo-3 and is subjected to a square depolarizing current.

Extension to Volumes and Deep Tissue

While epifluorescence microscopy provides a simple way to achieve high speed calcium imaging, this method can only be used at the surface of brain slices or in cell mono-layers. This is generally due to the fact that short wavelength excitation photons have a mean free path length of only tens of microns in typical brain tissues (Oheim). Many experiments can be done with epifluorescence to explore network properties, especially in homogenous networks. However for example in cortical circuits, canonical wiring diagrams distinguish different cortical layers, discrete layers of increased neuronal density which have widely different connections. Here, understanding how information is processed as it travels vertically from thalamic axons to higher integrating layers is something that manifestly requires sampling from volumes of intact brain tissue.

Laser scanning and confocal methods provide another way to implement fluorescence microscopy, and in particular 2-photon laser scanning microscopy (2PLSM) is particularly useful for penetrating deep tissue. These methods deliver structured illumination, while epifluorescence merely requires diffuse excitation illumination. Single photon laser scanning confocal microscopes deliver excitation by raster scanning a laser across the sample after focusing to a diffraction-limited spot by the aplanatic objective lens. Emission fluorescence is de-scanned by the same scanning mirrors which scan the excitation, and hence follows an identical returning optical path until separated by a dichroic mirror. The emission is spatially filtered by an aperture ideally the size of

one Airy disk, enhancing axial and lateral resolution by a factor of 2. Here detection is achieved by a single photomultiplier tube (PMT) rather than a camera, and position in the sample is translated to time at the PMT output.

Similarly, 2-photon laser scanning involves scanning femtosecond excitation pulses with high peak powers, generating non-linear excitation. Resolution is enhanced by a quadratic dependence of excitation on field intensity and photodamage and photobleaching is greatly reduced, but most importantly, due to the near-infrared excitation wavelengths used, diffraction-limited excitation can be achieved at depths up to 1 millimeter in intact brain. This allows live animals to be used for brain imaging, as chronic cranial window surgeries allow small rodents to be imaged over months, with the same individual neurons labeled with genetically encoded indicators.

To understand exactly how these modalities enhance resolution, it is helpful to examine some basic characteristics of their response functions.

Resolution in Fluorescence, Confocal, and Two-photon Microscopy

Spatial resolution in fluorescence microscopy is represented by the extent of the support of the three-dimensional frequency space representation (the optical transfer function OTF) of the point-spread function (PSF). In other words, the highest spatial frequency measurable indicates spatial resolution. This assumes point-wise linearity of fluorescence excitation and emission response, for example linearity of optical

photodetection, and independence and incoherence of fluorescence emitters. Invariance of the PSF over space is also assumed, which is approximately the case for planar imaging. The frequency content of any image is limited by the OTF, because any fluorophore density p(x,y,z) will be convolved by the PSF to yield the resulting fluorescence image, which results in a point-wise multiplication by the OTF in frequency space via convolution theorem. Only points which are non-zero in the OTF survive.

To understand how to image in three-dimensions it suffices to understand the factors contributing to the PSF and how it is generated. The response of a test fluorophore excited via dipole transition in the image plane of the microscope is given by the electric field intensity, which can be calculated in the scalar field approximation via the Fresnel-Kirchoff integral [9]. This part of the PSF is called the excitation PSF (ePSF). The resulting emission of the test fluorophore is averaged over dipole orientation, and combined with its ideal infinitesimal size it is appropriately equivalent to a spherical wave source--the Green's function for the Helmholtz equation. The sensitivity function of a detector in image plane due to this spherical wave after optical propagation is the detection PSF (dPSF).

The ePSF due to a focused plane wave or laser is proportional to the intensity of the field under the objective, in object space. This particular ePSF is useful for analysis of contrast generation, and ePSFs due to other types of illumination are generally degraded with respect to this. The extreme case is diffuse illumination, which has ideally no frequency content. Due to reciprocity in the Fresnel-Kirchoff integral, the

dPSF due to a spherical wave via the optical path can be approximated as this focused plane wave ePSF. Rather than use the scalar field approximation, this ePSF can be more precisely calculated in terms of time-averaged vector fields, with the result:

$$E_x = -iA(I_0 + I_2 \cos 2\varphi)$$

$$E_y = -iAI_2 \sin 2\varphi$$

$$E_z = -2AI_1 \cos \varphi$$

$$H_x = -iAI_2 \sin 2\varphi$$

$$H_y = -iA(I_0 - I_2 \cos 2\varphi)$$

$$H_z = -2AI_1 \sin \varphi$$

$$I_o \equiv I_o(kr, \theta; \alpha) = \int_0^{\alpha} cos^{\frac{1}{2}}\theta' sin\theta'(1 + cos\theta')\, J_0(kr\, sin\theta'\, sin\theta) e^{ikr\, cos\theta'\, cos\theta} d\theta'$$

$$I_1 \equiv I_1(kr, \theta; \alpha) = \int_0^{\alpha} cos^{\frac{1}{2}}\theta' sin^2\theta'\, J_1(kr\, sin\theta'\, sin\theta) e^{ikr\, cos\theta'\, cos\theta} d\theta'$$

$$I_2 \equiv I_o(kr, \theta; \alpha) = \int_0^{\alpha} cos^{\frac{1}{2}}\theta' sin\theta'(1 - cos\theta')\, J_2(kr\, sin\theta'\, sin\theta) e^{ikr\, cos\theta'\, cos\theta} d\theta'$$

$$A = \pi f l / \lambda$$

Where phi and theta are a spherical coordinate system centered at focus, J0, J1, and J2 are Bessel functions of the first kind, l is the incident electric field amplitude, f is the

focal length of the lens, (lambda) is the wavelength, k is the wave number, and alpha is the semi-aperture angle related to the objective lens numerical aperture (NA). It is convenient that the field intensity due to these fields (with different wavelengths) provides a basis for both dPSF and ePSF analysis. Figure 8 demonstrates the various modalities of fluorescence microscopy, and the resulting combined PSFs and OTFs are displayed in Figure 9-10.

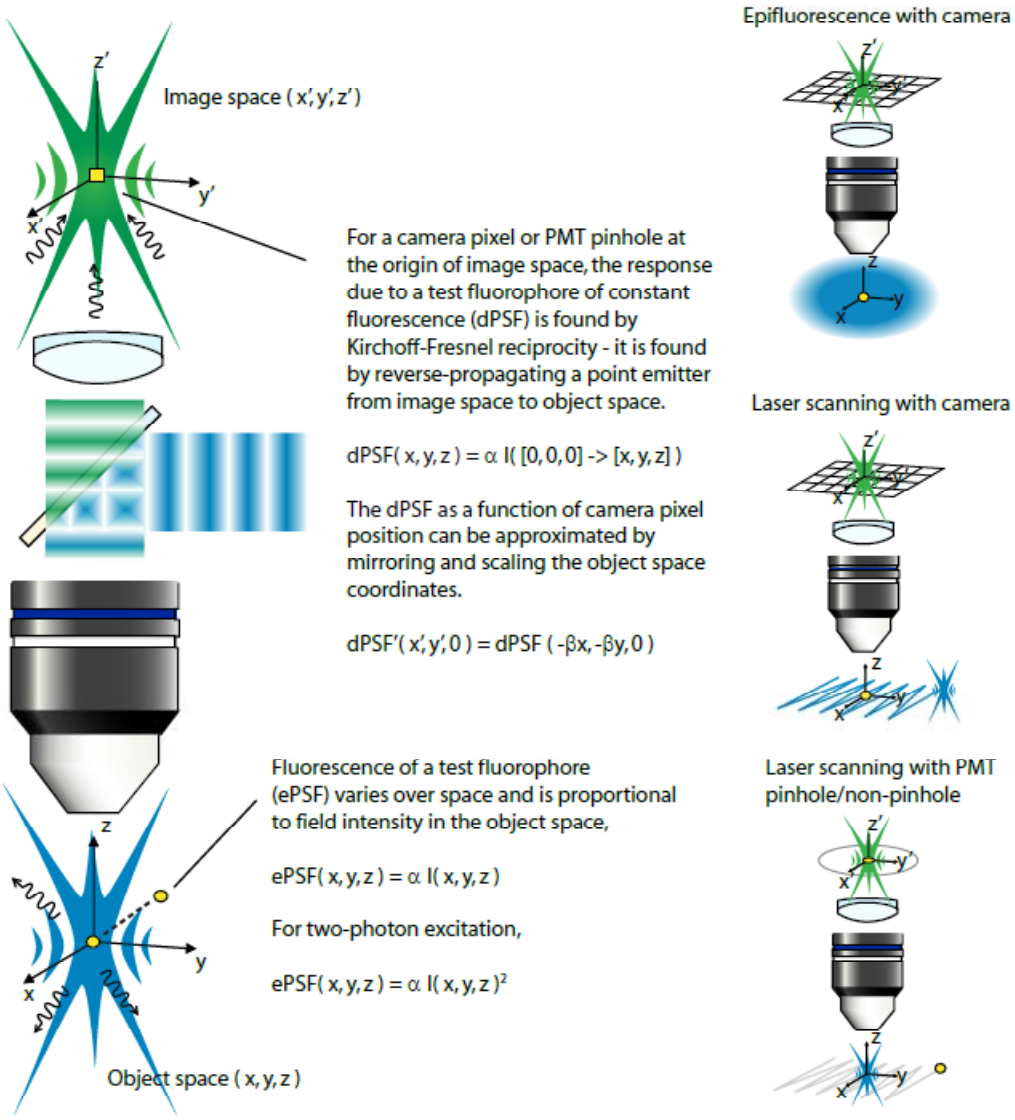

Figure 8

PSF coordinates are explained and various scanning configurations are illustrated

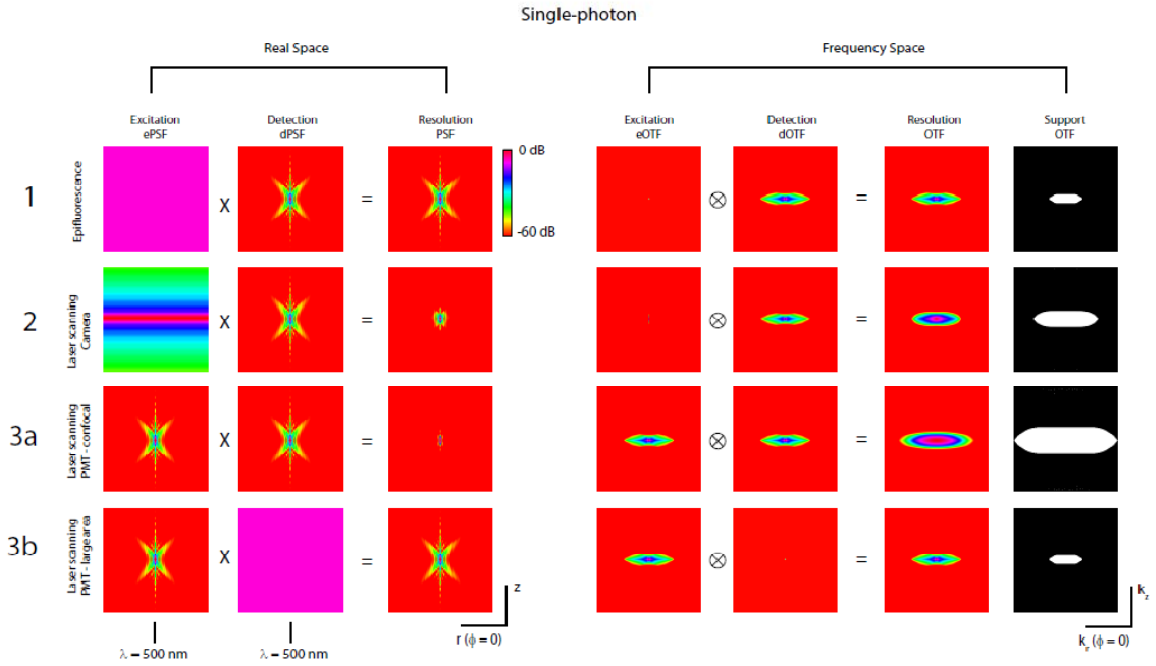

Figure 9

Resolution in various single photon fluorescence microscopy modalities

Resolution in various fluorescence microscopy modalities can be explored using the notion of spatially invariant dPSFs and ePSFs. Spatial invariance allows the equivalent use of frequency space (right side) as opposed to real object space coordinates (left side). The combined PSF is the coordinate-wise product of the ePSF and dPSF, and the Fourier transform of the combined PSF is the OTF. The non-zero extents of the OTF (the support) measure the resolution, as relative variations in the OTF can be adjusted for by frequency normalization (equivalent to deconvolution) if 3D data is available. Zeros in the frequency response cannot be recovered by post-processing.

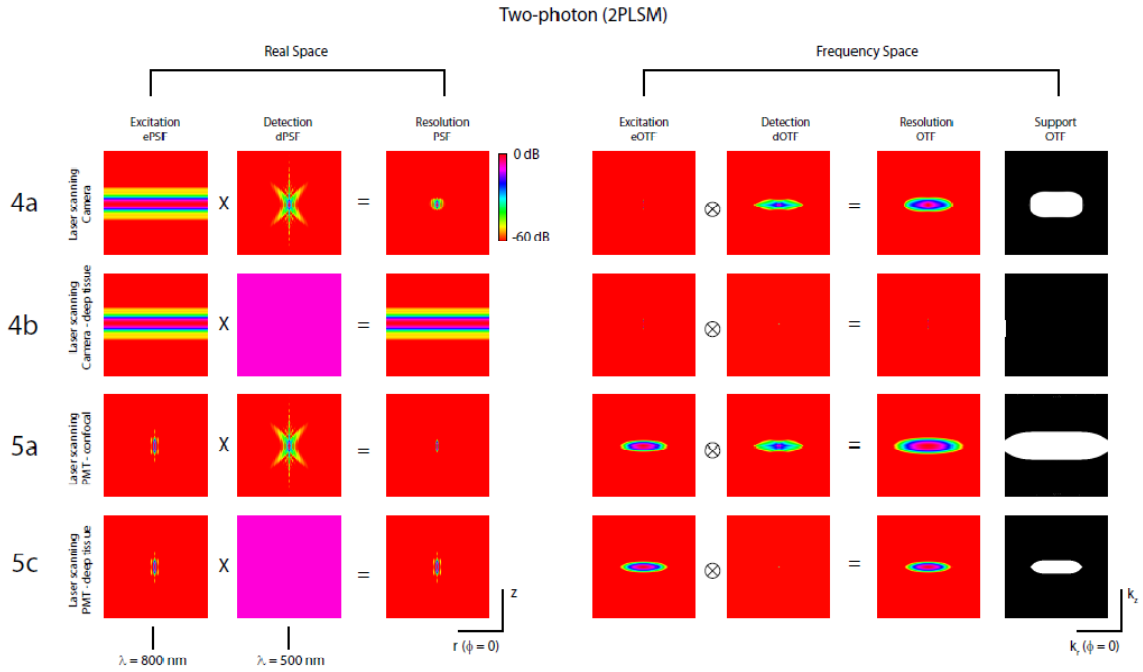

Figure 10

Resolution in various two-photon fluorescence microscopy modalities

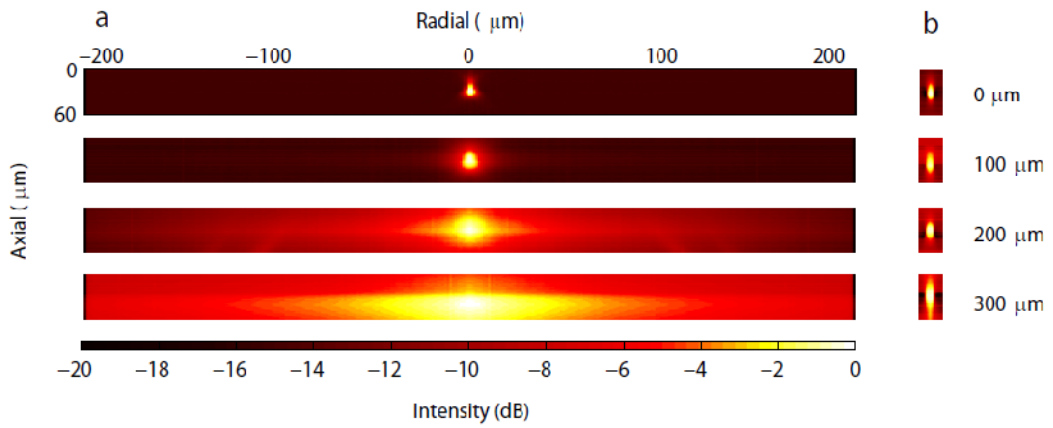

Figure 11

Effect of tissue depth on light scattering as measured by camera-type detection or photomultiplier tube

Combined point spread functions (PSF) measured as a function of brain depth. 5 µm fluorescein beads were placed under fixed brain slices of varying thickness and imaged with two-photon microscopy (single beam).(a) Degradation is seen in the camera-type detection case, caused by visible wavelength scattering. (b) As PMT-type detection is insensitive to degradation in the detection PSF, the combined PSF is only slightly affected.

1. Epifluorescence with camera detection

The dPSF is diffraction-limited due to imaging on the camera detector in the image space, and the ePSF is approximately a constant function due to the diffuse nature of the excitation, with ideally minimal spatial variation over the field of view. Contrast is completely due to the dPSF, and multiplication by the ePSF (convolution in frequency space) does not increase frequency content.

2. Laser scanning excitation with camera detection

In this case, the dPSF is still diffraction-limited. As each camera pixel is exposed for the entire laser raster scan, the effective ePSF is the convolution of the laser spot ePSF with the scan area. The result is similarly diffuse as in the case of epifluorescence, however there is a stronger z-dependence since this direction is not scanned, with high excitation in the focal plane.

3a, 3b. Laser scanning excitation with PMT-type detection (with or without pinhole)

This configuration is the case for traditional single-photon confocal microscopes. As the detector and the excitation laser spot are fixed relative to each other by optical

de-scanning, the test fluorophore can be considered scanned around their fixed geometry. The ePSF in this case is simply proportional to the stationary electromagnetic field intensity at focus, and when both the ePSF and dPSF are diffraction-limited, the combined PSF is roughly the square of the epifluorescence PSF, resulting in a doubling of resolution in all three directions as measured in frequency space. As the detection spatial filtering decreases (increasing pinhole aperture), the dPSF broadens until in the case of full PMT light detection, the resolution becomes equivalent to epifluorescence. However an important difference is that contrast is now due to the ePSF rather than the dPSF.

4a, 4b. Two-photon laser scanning excitation (2PLSM) with camera detection

In regions beyond the mean free path length for visible light, none of the single-photon modalities have contrast as the PSFs approach constant functions and the OTFs disappear. Due to the longer wavelengths used in the case of two-photon excitation, more than an order of magnitude is gained in depth due to the strong dependence on wavelength of scattering processes. However not all two-photon modalities will have contrast in deep tissue due to varying PSF composition.

In the case of 2PLSM systems, an epifluorescence-type diffuse illumination configuration is not feasible due to the high peak laser intensity required for the non-linear two-photon excitation process to be measurable. Thus excitation schemes are

limited to single or multiple point scanning, while both camera and PMT-type detection is available. The case of multiple pixel PMT-type descanned detection is not discussed here.

For camera detection, while the ePSF is now proportional to the infrared laser field intensity squared, the dPSF remains the same as in the case of single-photon excitation. For shallow samples, this leads to a similar result in the single-photon case, with the ePSF the result of stationary laser focused convolved with the scan path, and resolution is increased in the z-direction compared to epifluorescence, as well as gaining from the squaring of the stationary laser focus. The gain in resolution due to the non-linearity is not exactly double however, as it is canceled by the increase in the excitation wavelength versus single-photon excitation.

As with all camera detection schemes the combined PSF is highly dependent on the visible wavelength detection PSF. At tissue depths on the order of the mean free path length for visible light, the PSF is degraded considerably, and all resolving capability is lost.

4c, 4d. Two-photon laser scanning excitation (2PLSM) with PMT-type detection

When considering 2PSLM with PMT-type detection, with an appropriate pinhole aperture, similar to the case in single-photon excitation the resolution in the greatest. However in deep tissue, the resolution gain due to the ePSF and pinhole is lost, and to

collect more signal the aperture is maximized rather than minimized. The dPSF remains unaffected to depths approximately 8 times greater for example considering Rayleigh scattering, and within this range resolution is comparable to the case of single-photon epifluorescence. Of all the modalities presented, this is only one which allows any contrast in deep tissue.

Additional factors

Resolution is also affected by factors which degrade the translational invariance of the PSFs. such as linear absorption of excitation by fluorophores, which causes shallow out-of-focus fluorescence to be exaggerated. This particular effect is greatly reduced in the case of two-photon excitation, where fluorophore excitation is non-linear. Also in the case of two-photon excitation, taking into account the finite frequency bandwidth of femtosecond pulses and relative phase will make the description of the field intensity at focus more accurate, as each pulse comprises of a mere tens of cycles. A time-dependent description of the pulse at focus will produce different results for total fluorescence cross-section considering there is no time-averaging before squaring the field intensity.

Increasing the Speed of Two-photon Microscopy

As mentioned, illumination in two-photon microscopy is limited to laser point scanning. Using standard closed-loop scanning mirrors one can only record activity within a typical 512 x 512 image (a few hundred neurons with a 20X objective) at 1 Hz, which is not sufficient to reliably measure the exact timing of action potential spikes. For a fixed digitization rate (and, hence, fixed dwell time per pixel and number of laser pulses per pixel), scan rates can be increased by sacrificing vertical (y-axis) resolution. This comes at the cost of either reduced pixel dwell time per cell and line resolution per cell, or reduced field of view. Considering the finite line resolution required to identify cell contours for data analysis, temporal resolution of neuronal firing rates can be improved with 16 Hz scanning, but only a handful of cells can be monitored at once [10-12].

To overcome the slow scanning rate of closed-loop scanning mirrors, one approach is to simultaneously scan multiple beams across the sample, which reduces the time required to scan an equivalent number of lines or increases the field of view at an equivalent scan rate [13-16]. In such multifocal multiphoton microscopy (MMM), camera-type detection or de-scanned detector arrays are typically used to distinguish the fluorescence activated by the separate beams. Unfortunately, because the brain is a heterogeneous medium that greatly scatters and absorbs light [17], using this detection method the image signal and resolution degrade exponentially with depth (Figure 13). As demonstrated, camera-type detection systems rely on a diffraction-limited dPSF to generate contrast, while their ePSF is broad. This is the opposite of PMT-type detection systems, which have broad dPSFs and diffraction-limited ePSFs [16,18-19]. The result is that

it is not currently feasible to do high-speed in vivo calcium imaging deep with conventional MMM. In practice, MMM systems using cameras can only be used at depths less than the mean free path length for emitted photons in the tissue, typically 50-100 µm, such as dissociated neurons in culture or thin brain slices [20].

Spatio-temporal Beam Multiplexing for Preserving Imaging Depth

In order to achieve deep tissue MMM, we have adopted a method to distinguish fluorescence emission from different beams by separation in time that is therefore compatible with PMT-type detection (Figure 12). This method takes advantage of the shorter fluorescence decay time of synthetic fluorescent dyes (typically in the ns range) relative to the ultrafast laser repetition periods of pulsed lasers (tens of ns), which allows for additional time-separated excitation beams to be scanned simultaneously. This requires read-out electronics to assign fluorescence detected at different times to different portions of the image. The maximum number of beams that can be implemented is ultimately determined by the laser repetition rate and either the photodetector's time resolution or the fluorophore's decay time (whichever of the two is larger). In our prototype system, using a commercially available 80 MHz Ti:Al2O3 ultrafast laser, this translates into simultaneously scanning four beams that are separated in time by ~ 3 ns. Since our primary motivation was to achieve faster calcium imaging in vivo, we combined time multiplexing with a 16 kHz resonant scanning mirror

based system (although any scanning method can be used). This allows acquisition of 2-D images with 800 x 500 pixel resolution at 250 Hz, with a maximum field of view of ~500 µm x 300 µm (~100 - 200 cell bodies) using a 40x objective.

A unique capability of this spatio-temporally multiplexed MMM system is the ability to image multiple planes at distinct axial depths simultaneously without objective lens scanning or otherwise inertia-limited scanning. This is achieved by offsetting beam foci using simple lenses. Scanning with the same field of view and resolution as in the case of 2-D imaging, the acquisition rate becomes 60 Hz, capturing 100-200 cell bodies.

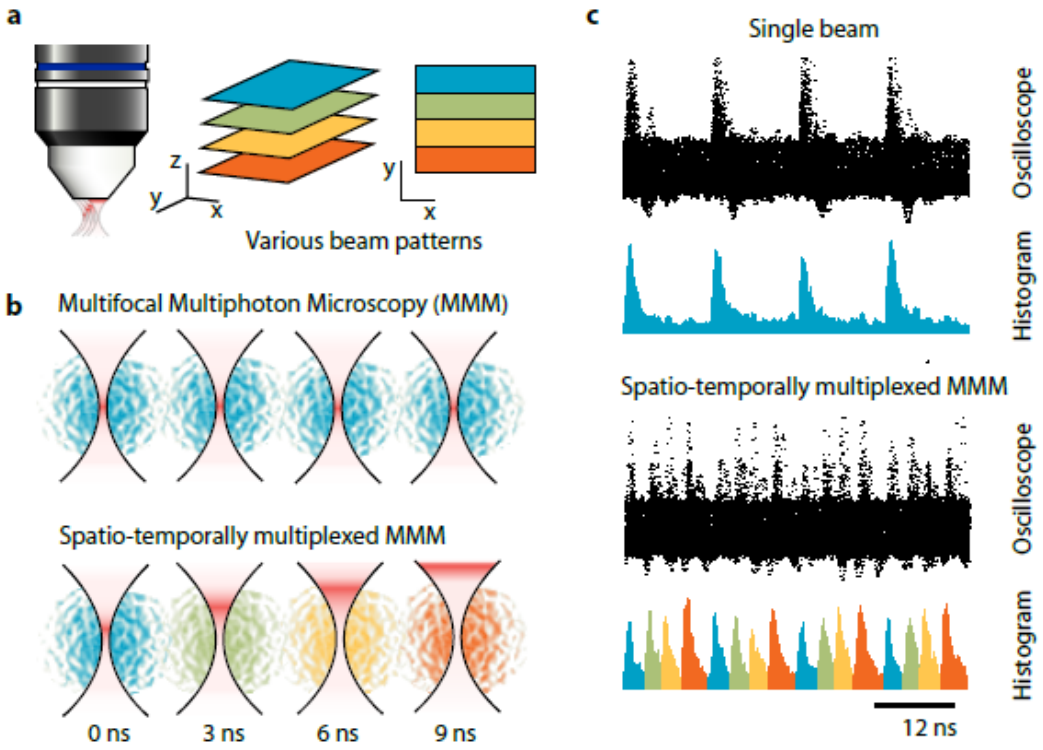

Figure 12

Spatio-temporal multiplexing to overcome depth limitations in MMM

(a) Cartoon of a microscope objective in a 4-beam spatio-temporal multiplexing system where 4 beams are successively delayed by the fluorescence decay time, allowing emitted fluorescence to be distinguished. Time multiplexing also removes ambiguity between different imaging planes, and allows both axial and lateral beam distribution. (b) Conventional MMM (top) and spatio-temporally multiplexed MMM (bottom). Conventionally, spatially distinct beams arrive at the sample simultaneously and emitted fluorescence is scattered and confused. With spatio-temporal multiplexing, each beam is delayed by 3 ns, which allows one to distinguish the emitted fluorescence from separate beams. (c) Time course of detected fluorescence signal. Overlay of 200 oscilloscope traces (top) and summary histograms (bottom) of single photoelectron events from a single 12 ns period excitation beam scanning a pollen grain. (d) Time course of detected fluorescence signal. Overlay of 200 oscilloscope traces (top) and summary histograms (bottom) of single photoelectron events from four beams spaced by 3 ns scanning the same pollen grain. Note that the fluorescence from separate beams can now be distinguished using the time resolution of the hybrid avalanche photodetector.

Spatio-temporal Beam Multiplexing

As 2PLSM involves pulsed excitation, it is naturally to consider the ways it can be time-multiplexed. In the case of 2PLSM, it so happens that spatio-temporal multiplexing of excitation pulses allows the ability of multifocal excitation in deep-tissue, without scattering ambiguity. Spacing between pulses is determined by the finite exponential fluorescence lifetime of emitted fluorescence, as when fluorescence from separate beams overlaps in time, it cannot be correctly associated with a specific beam. Spatio-multiplexing in 2PLSM not only allows multiple beams to be used in deep-tissue, but it allows a configuration such that each individual beam can be focused at different depths. This provides a general method for extending 2PLSM over a third spatial dimension with 100% observation duty cycle, and makes inertial objective lens axial

scanning obsolete. Thus one can imagine that in the future one speaks of image volumes being acquired, rather than single planes.

To construct the spatio-temporal beam multiplexing microscope prototype (Figure 13), we used simple optics to split the main beam from a 80 MHz Ti:Al_2O_3 laser (Chameleon Ultra II, Coherent, Santa Clara CA) into 4 spatio-temporally multiplexed beams with 3ns delays. Laser repetition rates can be decreased arbitrarily, allowing many beams in the future. The optical delays were designed for the fewest mirror reflections to aid alignment ease, but the footprint could be reduced using multiple reflections from fewer mirrors. Using polarization optics, the power of each beam can be controlled. The delayed beams were then converged on a conjugate plane of the objective pupil at the desired angle. Differences in optical propagation time of emitted fluorescence due to each beam were deemed negligible due to the short differences in distance traveled (millimeters) compared to the optical delays (meters). Importantly, during fluorescence emission from each beam, the photodetector remains sensitive to the entire collection area of the objective, which ensures that the sensitivity and resolution are equivalent to those of a single beam system (Figure 15).

Laser Scanning System

Our ultimate goal is to improve temporal resolution (or the size of the field of view with equivalent pixel dwell time) in 2-photon calcium imaging to achieve single

spike detection equivalent to electrophysiological recordings. Therefore, we sought to increase the frame rate above and beyond conventional closed-loop scanning mirror systems, while maintaining equivalent field of view and pixel resolution. In addition to scanning the sample with multiple beams, one can speed up imaging with a variety of fast scanning devices, including resonant scanning mirrors, piezoelectric and polygonal scanning mirrors, or acousto-optic deflectors (AODs). A comparison of scanning methods is presented in Table 1 (Appendix). For raster scanning systems, the maximum frame rate is determined by dividing the single line rate by the number of lines per frame (a 2 ms/line closed-loop scanning mirror acquires 512 x 512 pixel images at ~1 Hz). Once the fastest scanning method is chosen, the frame rate can only be increased by increasing the number of beams scanned.

For our prototype we incorporated a 16 kHz resonant scanning mirror (SC-30, EOPC, Ridgewood, NY) with a 3 mm beam aperture and 0.1 radian optical deflection. This is a conventional scan method that has been used previously for 2PLSM [21-22]. The resonant scanning mirror executes a bidirectional sinusoidal scan, producing a line rate of 32 kHz. We compensate for the non-uniform power delivery per angle and depth with an electro-optic modulator (MS-350, ConOptics, Danbury, CT). For the slow scan axis we used a closed-loop scanning mirror (6200H, Cambridge Technology). Custom electronics were designed and fabricated to synchronize the laser, scanning mirrors, electro-optical modulator (EOM), frame-grabber, and other components. With these components, our 4-beam system is capable of acquisition rate of 250 Hz with 800 x 500 pixel resolution.

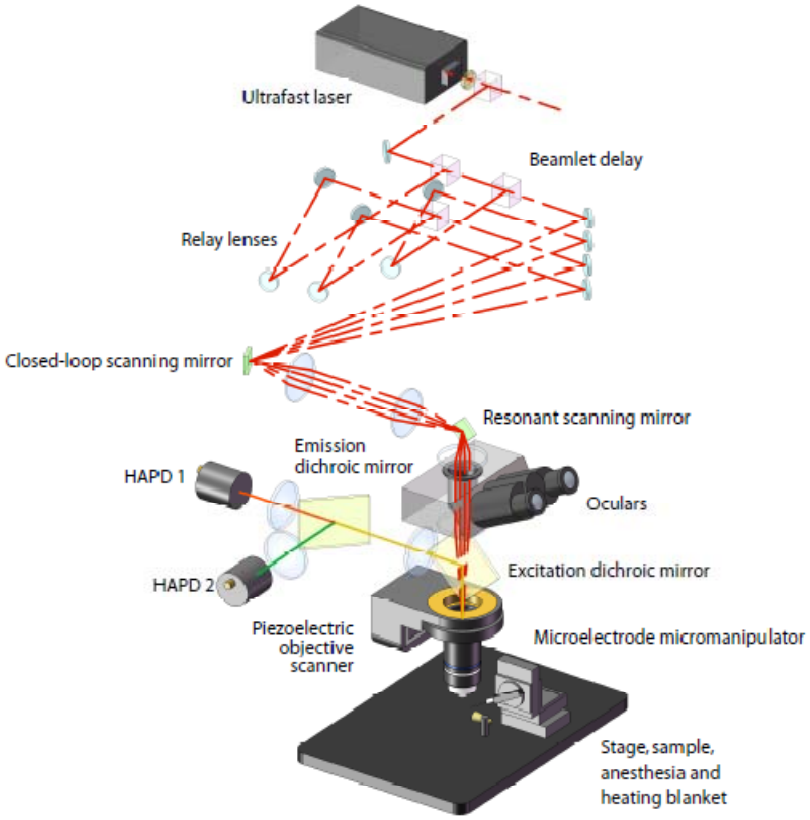

Figure 13

Spatio-temporal excitation emission multiplexing microscope prototype

Cartoon of the basic layout of the prototype microscope we used. Laser pulses are emitted with 12 ns period from the ultrafast Ti:Al_2O_3 laser. The beam is split into 4 beams using simple optics (beam splitting cubes), which are delayed by 3 ns each. The beams are eventually converged on the y-axis scan mirror aperture. The aperture is projected on to the objective back aperture. The resulting emitted fluorescence, which is highly scattered, is collected by two channels of HAPDs (for two separate fluorophores). The HAPD active area is placed in a conjugate plane of the objective back aperture, and is sensitive to a large sample area. For single plane raster scanning, the beams are converged at the desired angle onto the scanning mirror aperture.

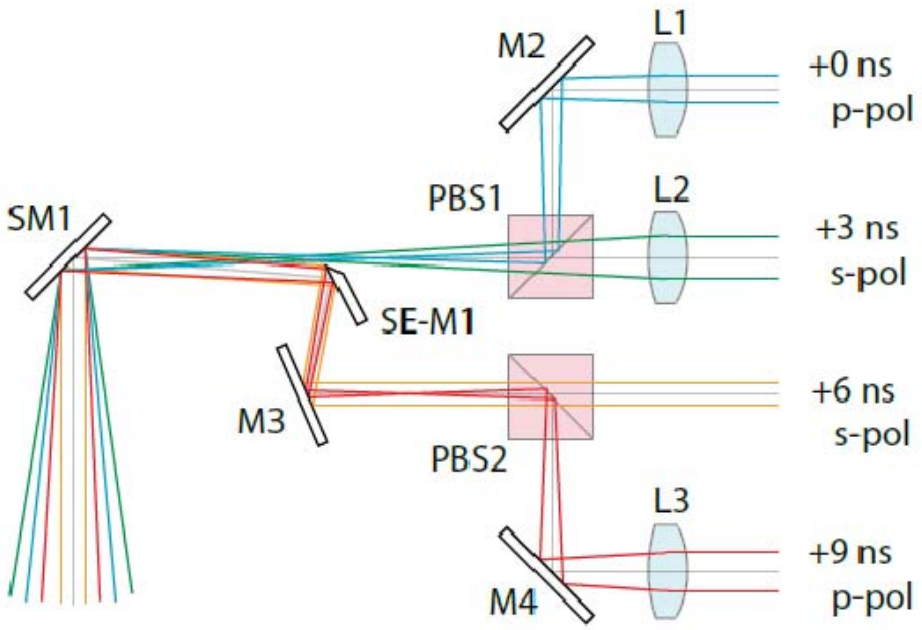

Figure 14

Optical configuration for multiple plane imaging

Spatio-temporal beam multiplexing can be used with any 3D arrangement of beams. To demonstrate multiple plane imaging, we used a slight modification of the optical path as compared to 2D imaging. Rather than converging beams with varying angle onto the scanning mirror (SM1), the beams were arranged as close to collinearly as possible, with varying divergence. Uniform back aperture filling was achieved by varying input beam diameter into three lenses (L1, L2, and L3) to ensure a common spot size on SM1. For two beams, colinearity was accomplished by polarizing beam splitters (PBS1 and PBS2). Further combination was achieved by sharp edge mirrors (SE-M1), but pinhole mirrors could also be used.

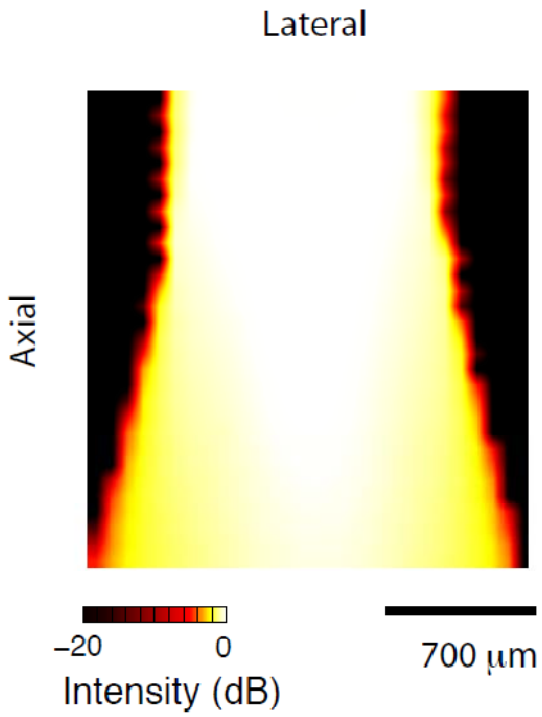

Figure 15

HAPD sample area sensitivity

HAPD sample area sensitivity, measured by scanning a spatially filtered green LED's 1 μm spot laterally and axially in the sample area, using a 1.2 NA water-immersion objective. For detection we used the same 40X 1.0 NA water-immersion objective as for in vivo imaging. Scattered light collection is maximized by placing the 3 mm diameter HAPD active area in a conjugate plane of the objective back aperture with an appropriate keplerian telescope.

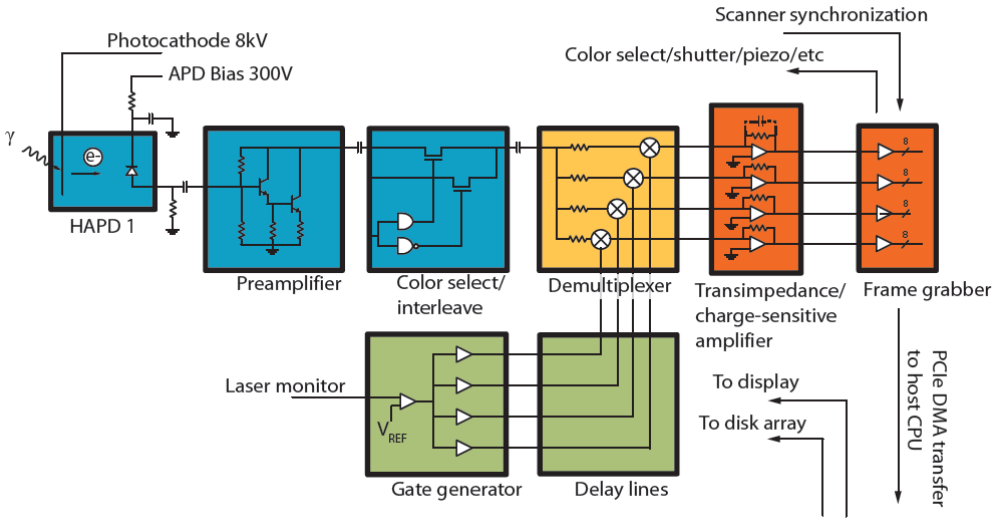

Figure 16

Read-out electronics

HAPD signals are amplified and color channel is selected or interleaved by a high-speed analog switch (blue). The signals from the four separate beams are de-multiplexed by four delayed gates with 3 ns width and 12 ns period (yellow). The delayed gates are generated by a laser monitor signal (green). The resulting current-voltage signal is then shaped for digitization by a four-channel high-speed frame grabber (orange). PCI-express DMA transfer allows for real-time display, processing, and disk array recording.

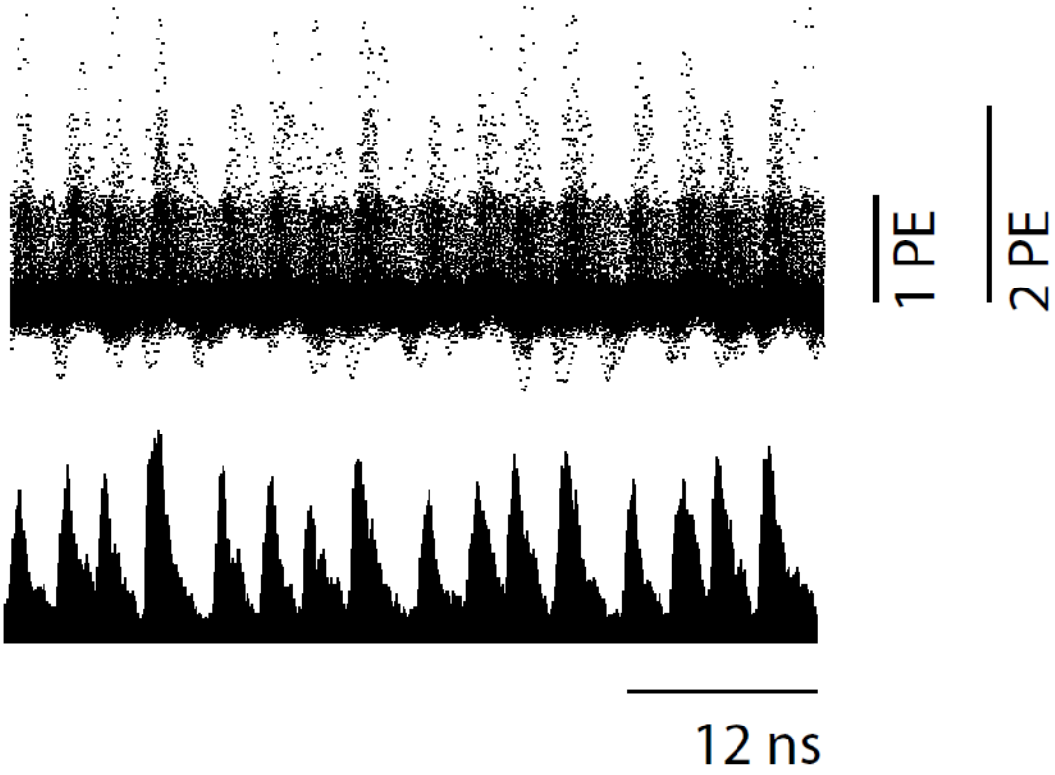

Figure 17

Oscilloscope traces of spatio-temporally multiplexed emission signal

De-multiplexing Fluorescence Emission

In order to de-multiplex fluorescence emission, a photodetector with a very short single photoelectron response (SER) time and transit time spread (TTS) is necessary. Traditional photomultiplier tubes (PMT) used for 2PLSM systems are inadequate because of their long SER pulse width and TTS (several nanoseconds each). Instead, we adopted a newer state-of-the-art photodetector, the hybrid avalanche photodiode (HAPD; Hamamatsu Photonics, Japan), which uses an avalanche photodiode as an electron bombardment target instead of the dynode stages of a PMT. The HAPD has a high first stage electron bombardment gain, which allows a low excess noise factor (a measure of the charge fluctuation of each SER) of ~1.0, as well as a high speed response (<1 ns) that is limited by the capacitance of the target APD [23]. While the HAPD's single photoelectron gain of approximately 10^5 is an order of magnitude lower than that of a PMT, the difference is recovered with a GHz preamplifier (Figure 16). This does not affect noise as this is dominated by the first-stage gain of the photodetector device, which is superior to conventional PMTs. The HAPD we used has a GaAsP photocathode with a 3 mm diameter active area and 45% quantum efficiency at 510 nm, which is nearly three times greater than that of multi-alkali photocathode PMTs. A comparison of candidate photodetectors for spatio-temporal beam multiplexing is displayed in Table 2 (Appendix).

Emission signals from the HAPD were de-multiplexed using 3 ns square demodulating windows that are synchronized with the laser pulses (Figure 16). This results in four separate signals that are shaped and amplified for subsequent digitization. This implies that our prototype system has the capability to operate as a fluorescence lifetime imaging (FLIM) system when used with a single excitation beam, using 3 ns wide gates in the time domain.

Image Display and Storage

After de-multiplexing and amplification, signals are digitized by a standard four-channel frame-grabber acquisition board (Helios eA, Matrox, Dorval, Quebec, Canada). Using two HAPDs and a fast analog switch, two colors can be switched or interleaved at the pixel or frame level and digitized by the same board. Signal levels are digitized at 8-bit precision per sample. We did not use the HAPD in a photon-counting read-out scheme to allow for high peak photon flux, but this is certainly possible given its fast response. Once digitized, the data is transferred across the PCI-express peripheral bus at sustained transfer rates > 700 MB/s and then displayed in real time. Display images are generally averaged to help visualize Fluo-4 labeled cells and neuropil activity. Geometrical horizontal distortion due to sinusoidal scanning distortion is corrected offline by linear interpolation resampling, or online with nearest-neighbor resampling. Imaging data are stored across a custom-designed high-bandwidth hard disk array with a maximum sustained transfer rate of 400 MB/s. This allows for two channels of data to

be recorded without interruption at roughly 100 MB/s at 10-bit resolution. Data can be continuously recorded until the disk array space is exhausted (~ 3 hours).

In-vivo Calcium Imaging

The primary purpose of our efforts is to further the realization of ideal in-vivo deep-tissue calcium imaging in the mouse brain. Ideally, optical methods such as calcium imaging would allow: (1) Cellular resolution, (2) Observation of three-dimensional ensembles, (3) Minimal tissue damage, and (4) Reliable action potential detection at high speed. The first three points are achieved by our prototype by maintaining typical in-vivo two-photon imaging parameters such as power, PMT collection , while the fourth is essentially a photo-statistical problem, limiting both speed and action potential resolution. It is important to note that the calcium indicator dye used is capable of single action potential detection with millisecond resolution as shown in the case of high-speed epifluorescence experiments, and our work is done

under the assumption that future improvements will allow ideal resolution by maximizing emission and collection photon flux.

To test our spatio-temporal multiplexing prototype, we carried out calcium imaging in live juvenile mice. This involves the performing of a cranial window surgery, replacing a small 3mm diameter area of the cranium with a cemented glass cover slip, allowing optical access to the surface of the dura mater. Before the cover slip is placed, (or afterwards, provided access) a few nanoliters of sulforhodamine 101 and fluo-4 AM calcium indicator dyes are slowly pressure-injected into the tissue for labeling (Figure 18). Ideally these calcium imaging techniques would provide diffraction-limited spatial resolution and millisecond recording of every action potential occurring in the imaging field, over hundreds of neurons. For the first time, we were able to carry out calcium imaging in-vivo over several different depths simultaneously, and while the temporal resolution in theory is increased with the introduction of multiple beams in deep tissue, in reality, these experiments await indicators which can deliver an order of magnitude more emission photon flux to increase the Poisson statistics-limited temporal resolution.

High-speed Imaging of Barrel Cortex in a Single Layer

Here, we demonstrate that we can use spatio-temporal excitation-emission multiplexing for deep tissue MMM and specifically for in vivo calcium imaging of neuronal activity in anesthetized mice. With conventional 2-photon calcium imaging

systems (closed-loop mirrors), temporal resolution (and spike detection) is improved at the expense of the field of view, such that one records the activity of only a handful of neurons simultaneously. In principle, using MMM with spatio-temporal multiplexing one can image a larger field of view (proportional to the number of beams) while maintaining the ideal pixel dwell time for optimal single spike detection.

We performed in vivo calcium imaging using standard Fluo-4 AM bulk loading protocols to monitor the activity of layer 2/3 neurons of somatosensory cortex in isoflurane anesthetized mice. With a 4-beam system, we could monitor the spontaneous activity of ~100 different neurons in barrel cortex at 250 Hz (Figures 19, 22). To identify cell contours for analysis, we used a combination of static and dynamic segmentation methods (Figure 19b; see methods in Appendix). These image processing algorithms demonstrate an advantage of high throughput full image acquisition versus point or arbitrary line sampling techniques (see Discussion). Next, we implemented established algorithms for temporal deconvolution of action potential-dependent calcium transients in neurons [8] to detect discrete events, from which we constructed raster plots (Figure 19e). Overall, the average firing rates derived from these deconvolved calcium traces for layer 2/3 neurons at postnatal days 15 - 21 (0.29 +/- 0.22 Hz) was similar to what we have previously reported using conventional 2PLSM with closed-loop mirrors [10]. To test the accuracy of the event detection in these deconvolved traces with respect to averaging over time, we compared deconvolved calcium traces filtered to different degrees and found better event detection with filtering at 25 Hz

than with filtering at rates equivalent to conventional 2-photon calcium imaging (Figure 19f). We also performed simultaneous patch-clamp recordings in cell-attached mode (Figure 22) and found that the simulated calcium traces convolved from the electrophysiology recordings closely resembled the actual calcium traces obtained from in vivo imaging (Figure 22e).

Simultaneous Imaging in Multiple Layers of Barrel Cortex

Next, we implemented slight modifications in the optics in order to be able to scan simultaneously separate axial planes with different beams. Beams were arranged collinearly, with a lens added for each beam to allow for focus offset while maintaining uniform back aperture filling. The four beams were spaced 30 μm apart from each other in the z-axis for a total pitch of 90 μm. This allowed us to monitor the activity of ~100-200 neurons distributed over a volume of layers 1 and 2/3 at 60 Hz (Figure 23), using the same in vivo calcium imaging conditions as in the case of 2-D imaging. In this case, resulting signal-to-noise ratios are reduced by a factor of 2 due to one-fourth the cell dwell time as opposed to single plane imaging of the same area. This was the first time calcium imaging had been performed in three-dimensional neuronal networks in vivo at high acquisition rates over appreciable depth.

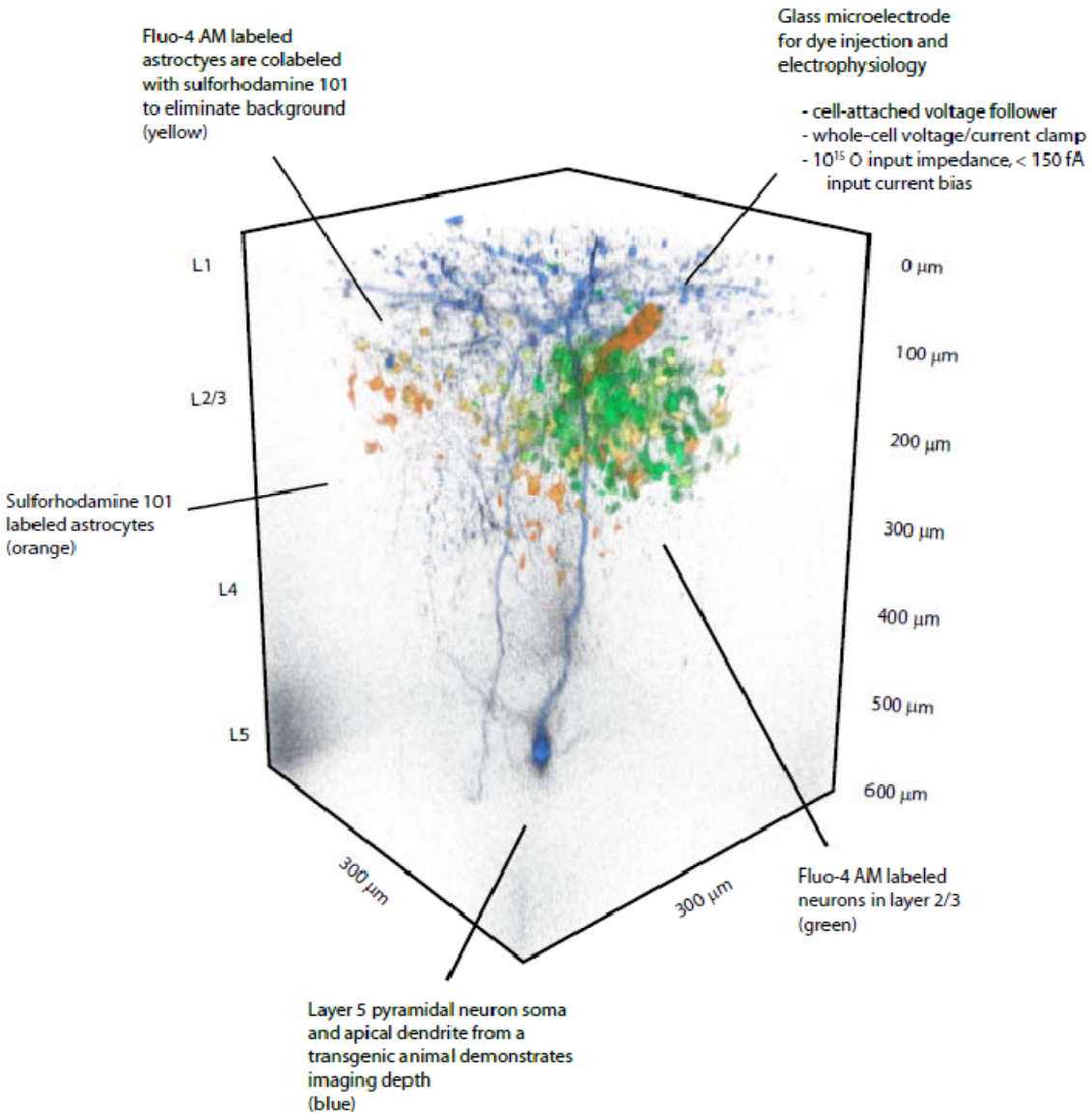

Figure 18

Summary of experimental methods and imaging environment

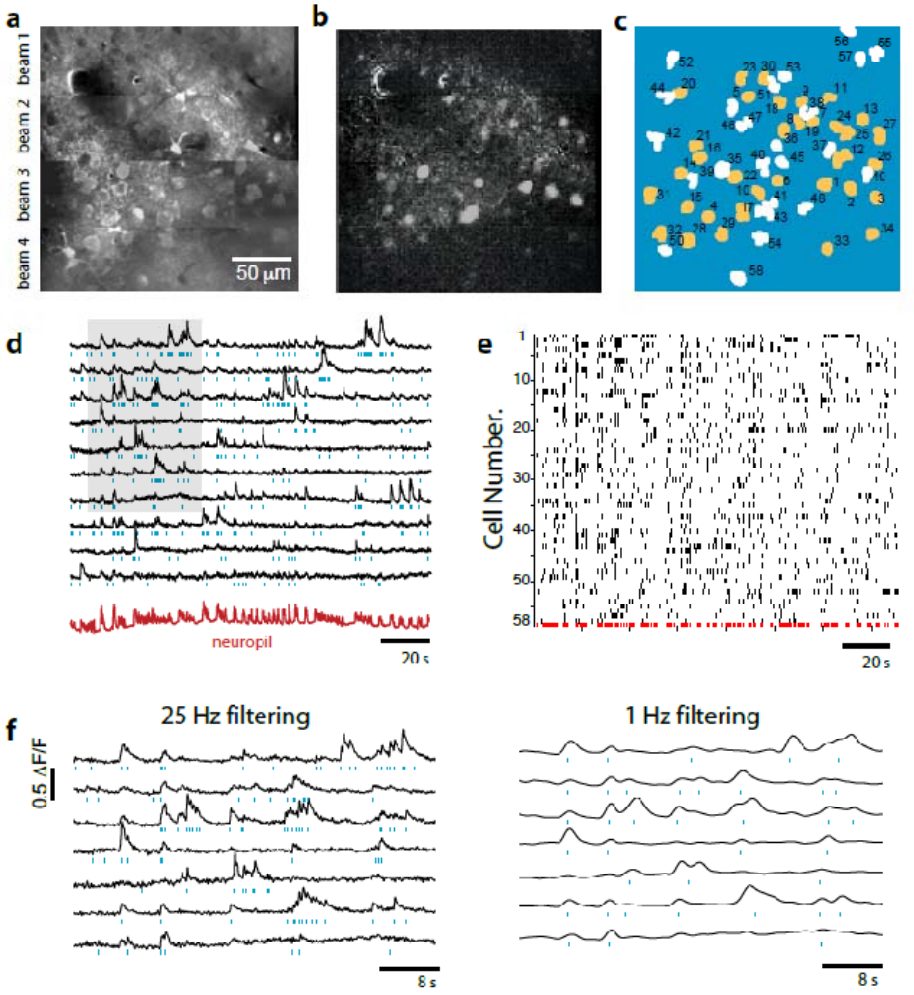

Figure 19

In vivo calcium imaging of layer 2/3 neurons in barrel cortex with spatio-temporal multiplexing

(a) Typical field of view scanned with 4 laser beams. (b) Segmentation into cell contours by dynamic detection method to capture active cells not readily seen in average intensity image. (c) Final segmented image of cells obtained through static (white contours) and dynamic detection (yellow contours) algorithms. The neuropil is shown in blue. (d) Raw calcium imaging traces of the first 10 cells shown with 25 Hz low-pass filtering. The neuropil signal is in red. The shaded area is shown with finer temporal resolution in *f.* Blue tick marks indicate calcium transients detected by a threshold of 2 σ in the deconvolved traces. (e) Raster plot of calcium events for all 58 neurons recorded. (f) Raw calcium imaging traces of the first 7 cells shown with 25 Hz low-pass filtering (left) and 1 Hz filtering (right).

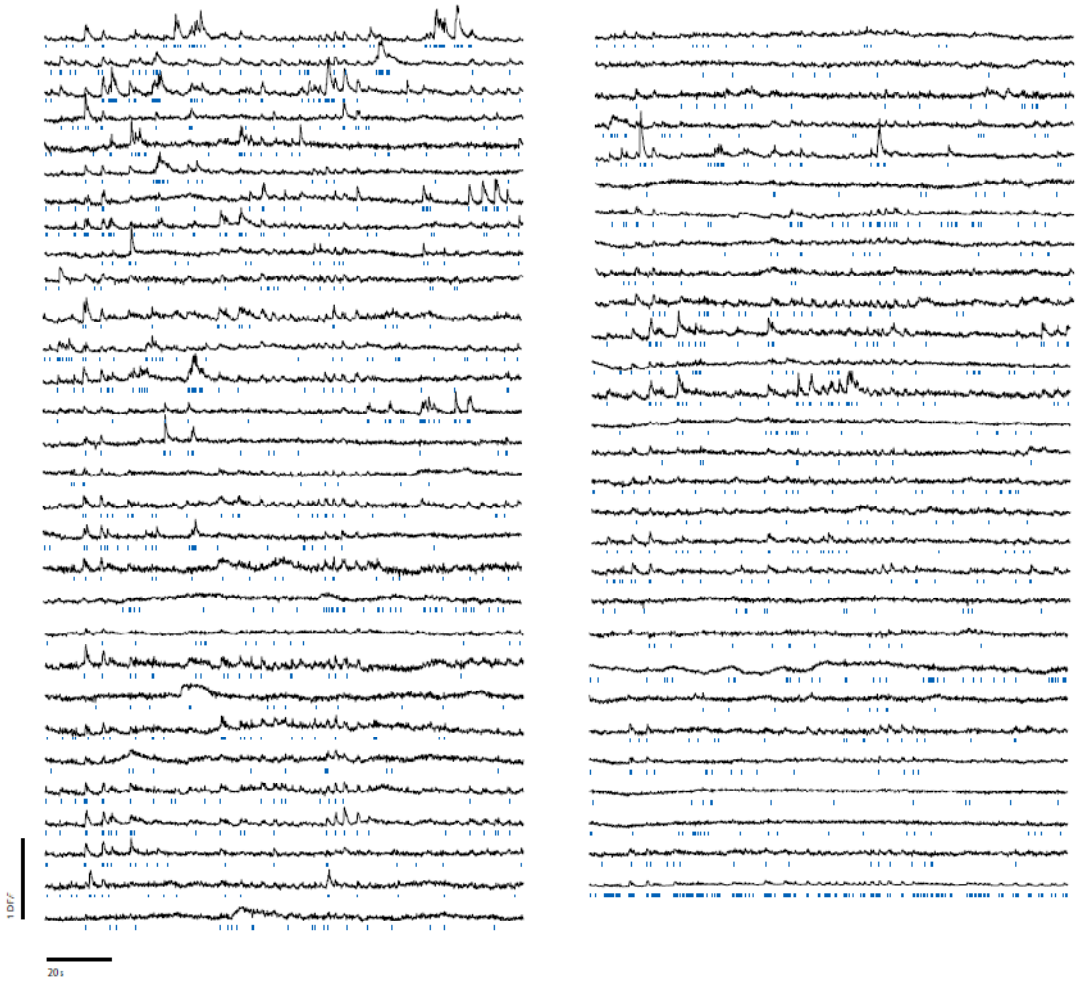

Figure 20

Raw calcium traces from all 60 cells in the field of view

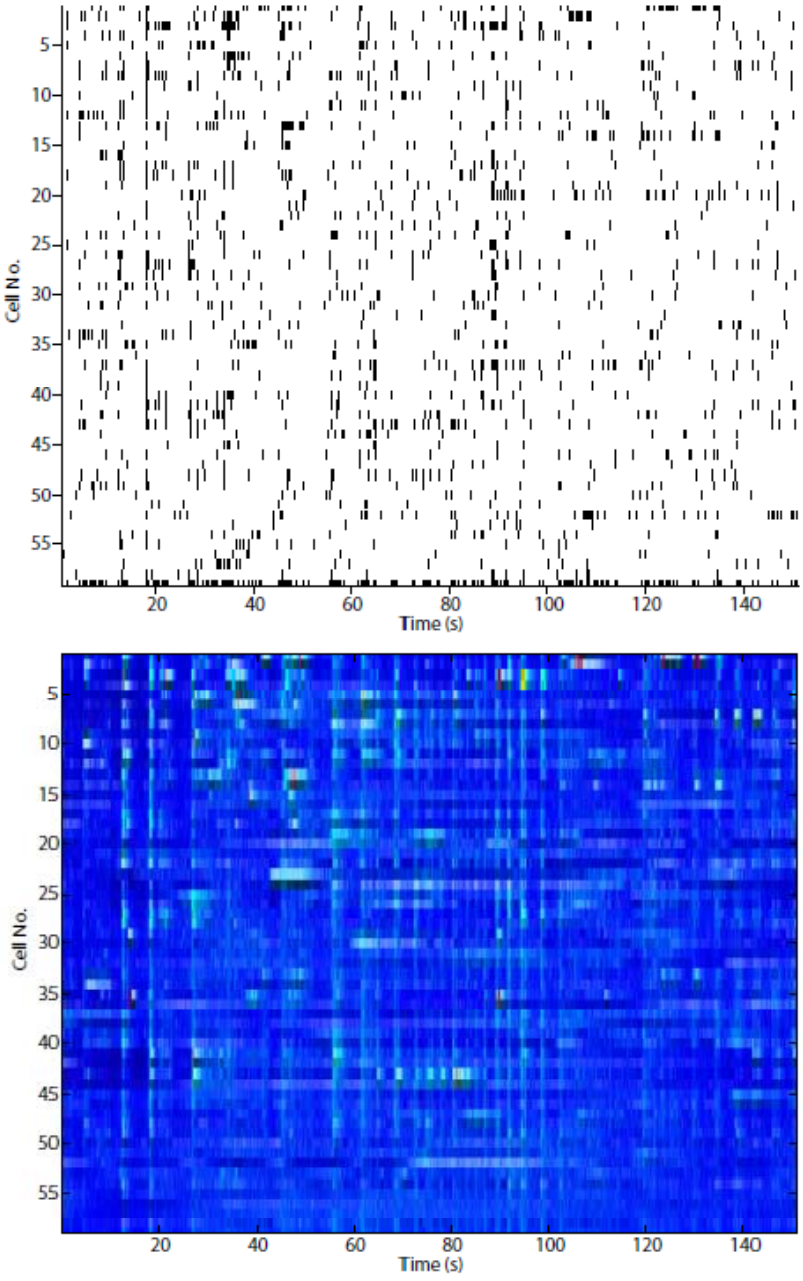

Figure 21

Raster plot of detected events and raw data from all 60 cells in the field of view.

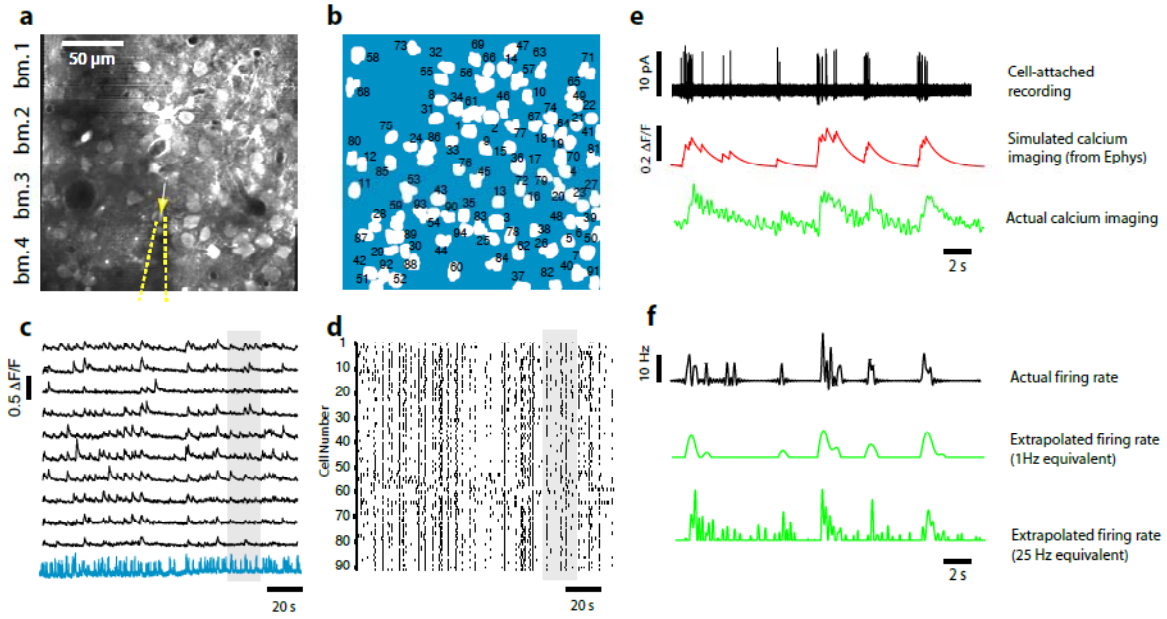

Figure 22

Multifocal in vivo calcium imaging and simultaneous electrophysiology

(a) Field of view scanned with 4 laser beams. The tip of the patch-clamp electrode is outlined in yellow and the recorded cell is indicated by an arrow. (b) Cell contours of 91 individual neurons automatically detected by the segmentation algorithm. Note that the algorithm does not detect all the cells and additional neurons could be selected manually. (c) Raw calcium traces from the first 10 cells. The simultaneous cell-attached electrophysiology trace is shown at the bottom (blue). The shaded area is shown with finer temporal resolution in *e*. (d) Raster plot of the calcium transient events for all 91 cells. (e) Detail of simultaneous electrophysiology and calcium imaging. From top to bottom: cell-attached recording trace (black), simulated (convolved) calcium imaging trace based on electrophysiology (red), actual calcium imaging trace (green)

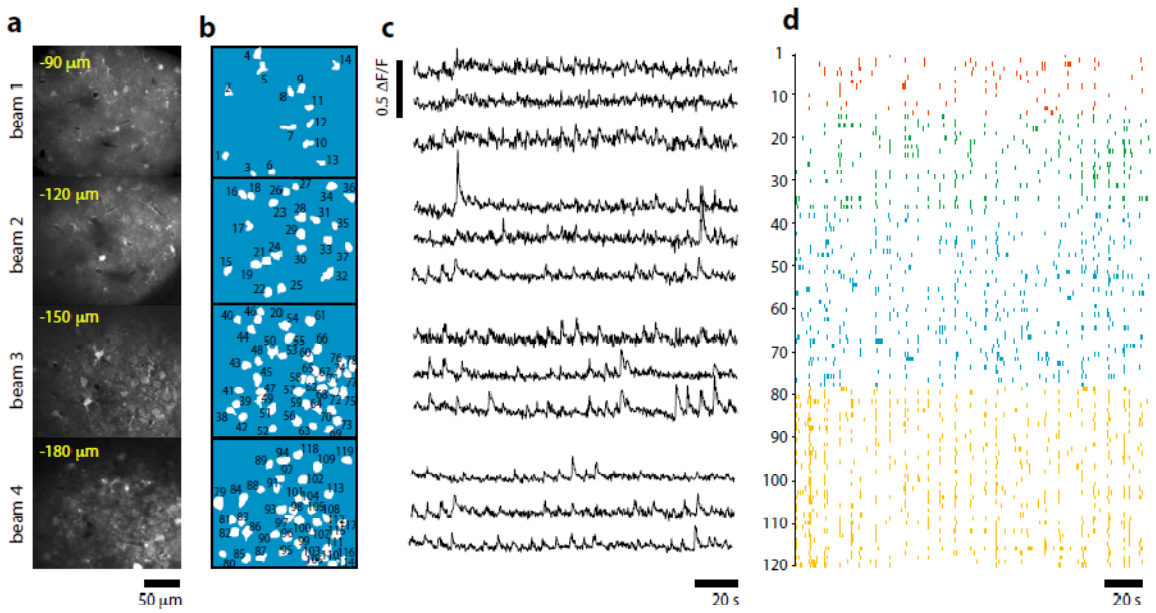

Figure 23

Simultaneous in vivo calcium imaging of neuronal activity in multiple axial planes with spatio-temporal multiplexing

(a) Field of view scanned with 4 laser beams. Note that each beam is scanning a different axial plane, spanning 90 µm, from layers 1 to layer 3 in barrel cortex. The depth of each beam from the cortical surface is indicated in yellow. (b) Cell contours of 120 individual neurons. A variable number of neurons were detected at different planes due to changes in cell density at different depths or signal to noise issues. (c) Raw calcium traces from 3 representative neurons per laser beam. (d) Raster plot of the calcium transient events for all neurons. Each color represents a different beam.

Discussion

2-photon calcium imaging is a promising tool for recording neuronal activity in vivo, because it is less invasive than electrophysiological recordings, more cells can be monitored simultaneously, and one can identify the cells being recorded (e.g., using genetically modified mice where subtypes of neurons are labeled with fluorescent proteins). Unfortunately, the time resolution of 2-photon calcium imaging has been limited by inherently slow raster scanning, such that accurate reporting of action potential firing is only possible for small groups of neurons in vivo [10-12,24]. Scanning multiple beams across the sample with MMM would increase the field of view for an ideal pixel dwell time, but in vivo calcium imaging with MMM has not been possible.

The temporal multiplexing technique we used provides an elegant solution to the problem of extending raster scanning MMM to deep tissue. In particular, we demonstrate how using a commercial Ti:Al_2O_3 laser, spatio-temporal multiplexing can be used for in vivo 2-photon calcium imaging to monitor the internal network dynamics of large ensembles of neurons. When scanning the sample with 4 beams in a single plane, we show that this approach can be used to record activity from ~100 layer 2/3 neurons and the firing rates we detect are comparable to what we previously reported using conventional 2PLSM and raster scanning at 4 Hz. Perhaps more importantly, spatio-temporal multiplexing also allows different beams to be scanned simultaneously at multiple axial planes [25], and we demonstrate for the first time simultaneous calcium imaging of neurons distributed over a depth of ~100 µm.

Increasing the number of multiplexed beams

The number of beams used in our system was dictated by the lifetime of the fluorophore being imaged, as well as the fact that the 700mm-1100mm asymmetric Ti:Al_20_3 cavity is the most common design commercially available (resulting in 80MHz being the common ultrafast oscillator base frequency). The calcium indicators OGB-1 and Fluo-4, with fluorescence lifetimes of ~0.5 and ~1 ns, respectively [26], are ideally matched to a 4-beam design using an 80 MHz laser, also considering beam splitting as occurring as powers of 2.

The most promising way to increase the number of simultaneous planes imaged to diffraction-limited axial sampling is to modify laser repetition rates. As limited maximum average laser power is a constraint, it is convenient that regenerative amplification and Bragg cell cavity dumpers provide a way to decrease repetition rate from 10MHz to kHz, while maintaining average power. For example, Bragg cell-based cavity dumpers use AODs to modulate the output coupling of the laser cavity, allowing integer multiplication of the fundamental laser period. One would like to use this flexibility to realize the optimum combination of initial repetition rate, number of multiplexed beams and beam time-separation, and total average power or energy per pulse. A typical case might be 1MHz initial repetition rate split into 20 beams, with 20MHz final pulse rate. Each beam would be separated by 50ns, providing ample resistance against beam cross-talk due to fluorescence lifetime. In this case, for a 4 W laser, energy per pulse would be 50 nJ. Higher energy per pulse is always desirable, as the group of Winfried Denk has demonstrated in-vivo imaging with mJ order pulses (for the deepest layers where exponentially degraded focal energies must be maintained at reasonable levels)[27]. However the tradeoff of decreasing repetition rates is decreased horizontal sampling rates. For a 20MHz final sampling rate with 20 beams, each plane would be sampled at 1MHz pixel rate, with a 256 x 256 x 20 volume acquired at 16Hz.

Ultimately, where acquisition rate meets photo-statistical limits (ie energy per pulse and two-photon excitation efficiency) defines the optimum parameters. Acquisition rates which do not lead to energy per pulse high enough to yield enough

photons are not useful. We do not attempt to construct these curves here, as they are dependent on relevant fluorophore yield per pulse, collection optics, non-ideal loss through regenerative amplification or cavity dumpers, attempted imaging depth, desired system cost, etc. Achieving a reasonable approximation to optimum parameters should be a priority in the in vivo two-photon calcium imaging community.

The current state of in-vivo two-photon calcium imaging

Several different scanning configurations are currently available for in-vivo two-photon calcium imaging. Aside from traditional raster scanning, these most notably include acousto-optic deflector (AOD) based scanning, and arbitrary line scanning. These latter two methods introduce a means of increasing the cell duty cycle—a measurement of the ratio of time spent on cells to the time spent on local background neuropil. Duty cycle and scanning method aside, all two-photon calcium imaging systems seek to be purely photo-statistically limited. Given a laser repetition rate and a pulse energy, the total photon flux should be relatively fixed. Typical numbers might be 10MHz photon rate for an 80MHz laser repetition rate with 10 nJ per pulse, and this may allow on average 1 photon per pulse to be observed. Then, given 10 million observed emission photons per second, distributing them among scanned cells yields a total number of observable cells at a given Poisson noise level and time resolution. For 3% noise (1000 photons per time point) and 100 cells, the maximum time resolution is

10 ms (100Hz) (note that a single action potential causes an approximately 10% increase in fluorescence with Fluo-4). This effectively summarizes the current state of in-vivo calcium imaging: The maximum possible performance is limited to these numbers, regardless of scan method, unless light throughput is increased. Our contribution here allows these 100 cells to be distributed over depth, for the first time.

Monitoring 100 cells with single action potential resolution at 100Hz would be considered ideal, and we did not reach this limit here. As mentioned, to reach this limit, several things must be true: (1) readout noise must be zero (ie some type of photon counting must be used) and (2) cell duty cycle must be 100%. The second requirement is compromised in the case of full image acquisition, as dark areas must be raster scanned to aid image interpretation. Use of AODs allows the duty cycle to reach 100%, with several tradeoffs not mentioned here. The first requirement calls for charge-integrating electronics or photon-counting electronics. Photon-counting electronics limits the maximum possible photon flux as a single channel PMT can count at a finite rate due to photo-electron pulse width. This could be remedied by a more sophisticated readout scheme using a multi-anode detector. We hope that photon counting readout becomes more widely adopted, and one reason it is not is that non-calcium imaging operation involves high peak count areas such as GFP-labeled processes. To accommodate higher count rates one of our short term goals is to develop multi-pixel or multiple photoelectron quantizing photodetector readout, to read in excess of 1-10 Giga-photons per second.

Once readout noise is minimized and duty cycle is maximized or compromised, performance can only be increased by increasing light flux. One worthy approach is to consider optics in addition to the objective lens to aid collection of the 2π solid angle available to the experimenter. However more importantly, the upper limits of excitation power, both average and peak, must be explored (see Figure 31 in Appendix). This includes exploring photo-damage limits as well as the development of higher power table-top ultrafast lasers. As far as damage limits, some popular studies indicate low peak power damage thresholds at low depth[28], and orders of magnitude higher thresholds in deep tissue[27]. Electro-optic Modulators (EOMs) provide a way to attenuate power at different depths, so the only concern here should be how to make more power available in a table top system. In commercial systems with the highest average powers (several watts), power is limited by the solid state Nd:YAG 532nm pump power, which is in turn limited by infrared laser diode pump power of approximately 20W. It is hopeful that increasing power and increasing pulse energy in the future will provide both more spatio-temporally multiplexed beams as well as more emission photons. In the near future we hope to achieve 1GHz emission photon rates, providing perhaps 1000 observed cells and 1 ms time resolution, allowing the dynamics of entire cortical columns to be measured with the aid of multiple plane imaging.

Finally, improved calcium sensors will allow less stringent requirements on the number of photons allotted per frame per cell for single spike detection. The number of photons freed will be proportional to the square of the noise requirement relaxation.

The development of improved calcium sensors might be more demanding than power, optics and readout electronics improvements however.

It is not so unlikely that in the near future, ideal two-photon calcium imaging in vivo is realized. Using the case of our initial epifluorescence experiments, detection of action potentials with millisecond resolution optically is possible. To be able to achieve this in-vivo, and to be able to probe three-dimensional tissue non-invasively would enable a greater understanding of information processing in working cortical networks. We hope our method of spatio-temporal multiplexing with hybrid photodetector and readout electronics helps to build towards this goal.

Appendices

Materials and Methods

All chemicals were purchased from Sigma-Aldrich unless otherwise stated. All experiments were performed under animal protocols approved by the Animal Research Committee and the Office for the Protection of Research Subjects at the University of California, Los Angeles.

Constructing a laser scanning microscope

Constructing a laser scanning microscope is relatively fast and inexpensive. The overall design can be seen as a combination of a few simple components. The overall goal of a laser scanning microscope is generally to scan a TEM_{00} laser beam across a microscope sample after focusing by a microscope objective lens. Due to the availability of lenses, scanning mirrors, filters, optomechanical parts, mechanical stages, and structural components from prototype and lab equipment vendors, parts can be acquired quickly with minimum custom fabrication or machined parts. After laser scanning, photodetection of fluorescence is necessary, and this requires a PMT-like photodetector with associated optics, separated from the laser scanning system by a dichroic mirror. Many interchangeable photodetectors could be used, available from companies such as Hamamatsu Photonics K. K., from optics distributors such as Edmund Optics. In addition to scanning and detection sections, the microscope should also consist of an appropriate sample stage and focus drive.

The laser scanning microscope is usually placed in a room with controlled lighting and air-conditioning. Since microscopes are sensitive to minute mechanical vibrations (especially at the stage and sample) which introduce relative motion between the sample and other components, a quiet room and a floating vibration isolation table are required. Such vibration isolation tables are available from companies such as Newport SpectraPhysics Inc. The optical variety include an array of tapped mounting holes for

mounting optomechanical parts. Additionally, a circulating air filter can be included to reduce dust accumulation. Especially the smallest particles tend to limit the lifetime of optical components.

For mammalian in-vivo imaging via window craniotomy, an upright-type microscope is desired, as opposed to lateral or inverted geometries. This geometry involves the microscope objective being lowered onto the sample from above, and this generally allows samples which are large or 3-dimensional rather than thin slide-mounted samples. This allows for the window craniotomy to be accessed from above, with injection and electrophysiology glass micro-electrodes to be advanced from above as well in the same manner as the microscope objective approach.

On the vibration isolation table, because a somewhat planar and large optics prototyping area is desired, an upright laser scanning microscope requires that a platform be mounted on the table, with the microscope objective and photo-detection portions of the system mounted vertically off the side. We chose a platform of several feet by several feet, mounted at a height of 600 mm. This has a disadvantage of the optical plane being at a height close to typical eye-level, however careful application of thick laser shielding and laser dumping can be used. As ultra-fast laser pulses can non-linearly damage and ablate materials without heating them, even when using low average powers, over long periods such as months laser shielding should be inspected for any degradation at unprotected hot spots. Hot spots should be blocked by

reinforced scattering and absorbing beam dump components. Hot spot occurrence should be rare due to the desire for high optical beam efficiency.

For laser scanning systems and most optical systems, rigid mounting for fixing the optical train is important. For ultrafast laser systems, whose pulses suffer temporal dispersion after fiber-optic delivery, direct mounting of the laser head without use of fiber-optics is necessary. In other words, direct beam steering must be used to guide the laser into the system, unless specialized dispersion compensation is used. Pump lasers, power supplies, and chillers can be placed above or below the table, with umbilical cord and pump laser delivered remotely. Ultrafast laser systems require threshold powers to be reached to enable passive Kerr lens mode-locking (KLM), and hence run at constant pump and output power. This requires a separate polarization optics section to passively modulate power at the laser output. Unused power should be delivered to a beam dump component or laser power meter.

While rigidly mounting should keep the laser output beam pointing direction relatively constant, changes in laser cavity conditions and pump laser steering can cause drift in beam pointing. In the laser scanning microscope, this is amplified by additional mirrors and optical components. It is important to have a method for compensating for laser pointing drift which allows for at least four degrees of adjustment. These four independent (but not necessarily orthogonal) degrees of freedom are required to define beam origin and pointing angle into the system. Inexpensive beam steering feedback systems with positional photodetectors exist for this purpose, however for lower cost

systems, a set of two calibration apertures set as far apart as possible allow for laser pointing drift to be compensated manually at regular intervals by user.

Scanning Section

Once a path for steering the laser beam into the laser scanning system is well defined, an optical system is constructed to achieve optical beam scanning, raster or otherwise. A variety of scanning devices are available. However generally they require placement in infinite conjugate space relative to the microscope optical train, where different points in the sample correspond to different angles of TEM_{00} beam projection. Further, it is generally required for sample points to have laser focus occur with equivalent numerical aperture, with the incoming laser beam to approximately fill or be fixed in the microscope objective pupil and back aperture. As lenses will propagate TEM_{00} beams in a manner similar to but in an exactly equal way as predicted by geometrical optics, the required positions of any laser scanning devices can be calculated by following the conjugate planes of the objective pupil and back aperture backwards through the optical train. Further, as TEM_{00} beams will generally require only correctly aligned Galilean or Keplerian telescopes to maintain their beam profile, the configuration of lenses used in the laser scanning system optics is highly constrained. In particular, for back propagating the objective pupil and back aperture

images, only the Keplerian telescope is useful, as it projects images a positive distance backwards, whereas a Galilean telescope projects a virtual image.

Thus in general, for laser scanning microscopes, starting from the objective, optics will consist of lenses spaced by the sum of their focal length and the focal length of the preceding lens. Keplerian telescopes consist of pairs of these lenses, and their ratios are designed to contract or expand beam diameters, and correspondingly amplify or attenuate scan angle. These Keplerian telescopes project the image of the back aperture, with a different scanning mirror or spatial light modulator (SLM) placed at each one.

Many different scanning devices are available, and have varying mirror aperture, scanning angle, operating bandwidth, mirror coating and flatness, etc. For devices such as polygonal scanners or diffractive devices such as electro-optic or acousto-optic deflectors (AODs), time where the beam aperture is occluded must be taken into account. For devices such as resonant scanners operating frequencies can be externally fed and locked to via phase-locked loop (PLL) however this sacrifices amplitude generally. For example, one generally may want to lock a resonant scanning period to a multiple of the laser frequency. Some devices may be quoted a limited number of diffraction-limited points which can be scanned, however this is generally assuming specialized conditions and can be ignored in some cases. See Table 1 for a comparison of scanning devices.

One can take the quoted scanning angle of a device in radians and multiply it by the focal length of the objective, adjusted by any intermediate telescopes, to obtain an estimate of the scanning field of view.

For a given set of scanners, a solution for synchronizing and driving them must be devised. This generally requires output command waveforms to be generated or read by high impedance input or output lines to and from manufacturer supplied electronics driver boards. One simple way to implement simple repeated digitally synthesized command waveforms is to use a general purpose digital acquisition system (DAQ) for example from National Instruments. This allows an onboard reference clock or other signal to be used as a master clock for signals generated. For example, a resonant scanner signal may need to serve as a clock to generate a closed-loop galvanometer signal. Auxiliary signals may need to be generated, and examples of the architecture and assembled control circuits for the spatio-temporal multiplexing prototype are shown in Figures 27 and 28.

Detection Section

To detect signals, one uses a separate detection pathway separated via a dichroic mirror. As ultrafast laser pulses have associated non-linear damage, and dielectric coating filters and mirrors have high incidence angle dependence, care must

be taken to guard sensitive photodetector equipment from the separate laser scanning pathway. While absorptive filters can be used, transmission for these filters cannot be tuned with the same control as reflective filters. The goal of the detection pathway is to route as much signal as possible to the photodetector. For 2PLSM systems, this involves projecting the back aperture of the microscope objective onto the photodetector active area with minimum loss. Detection optics must be designed appropriately, particularly with wide optics. Wide optical trains also allow generally for less angular divergence, which is beneficial for filter incidence angle.

For 2PLSM systems, the smallest acceptable photodetector area is approximately the same size as the effective emission area in the sample. The relevant optical train and optimization is similar to that for a high-intensity microscope condenser, with 1:1 projection providing optimum collection. To reach this optimum, a high NA condenser is also required close to the photodetector.

A comparison of photodetectors is presented in Table 2, however specifically for spatio-temporally multiplexing or time-correlated single photon counting (TCSPC) sytems, in addition to photodetector area and quantum efficiency (QE) a short photodetector transit-time spread (TTS) is required (and also short single photoelectron rise time in the case of non-photon counting readout). The TTS is the dominant contribution to photoelectron timing accuracy.

For high-throughput and high-bandwidth systems as is the case with the spatio-temporal multiplexing prototype, RF bandwidth must be carefully managed throughout

the detection electronics pathway, starting from the photodetector preamplifier and ending with the analog-to-digital converters (ADCs). In the spatio-temporal multiplexing prototype, AC-coupling is used, reducing the accuracy of low spatial frequency photocurrent measurements. All stages have -3dB bandwidths of at least 2GHz, and in most cases 8GHz. This is especially true for the analog demodulation stage, which must carry an approximation to a square 3 ns pulse for assigning fluorescence from different beams to the appropriate digitization pathways. Demodulation at this stage is accomplished with an analog RF multiplier chip operating from DC-2GHz (ADL5391, Analog Devices) in a custom RF printed circuit board. For a schematic and assembled circuit for spatio-temporal multiplexing prototype demodulation, see Figures 29 and 30.

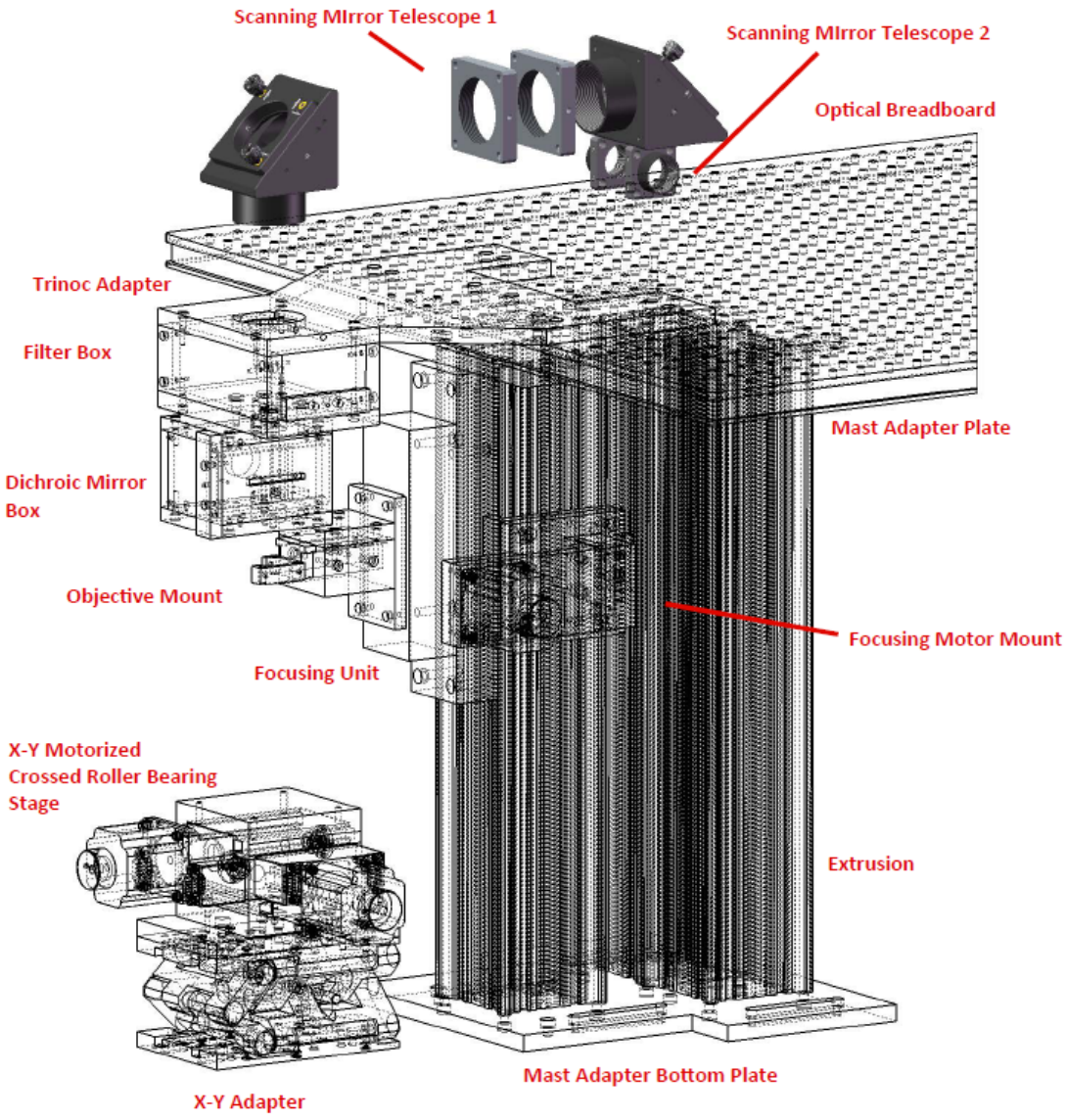

Figure 24

Spatio-temporal multiplexing 2PLSM microscope prototype optomechanics

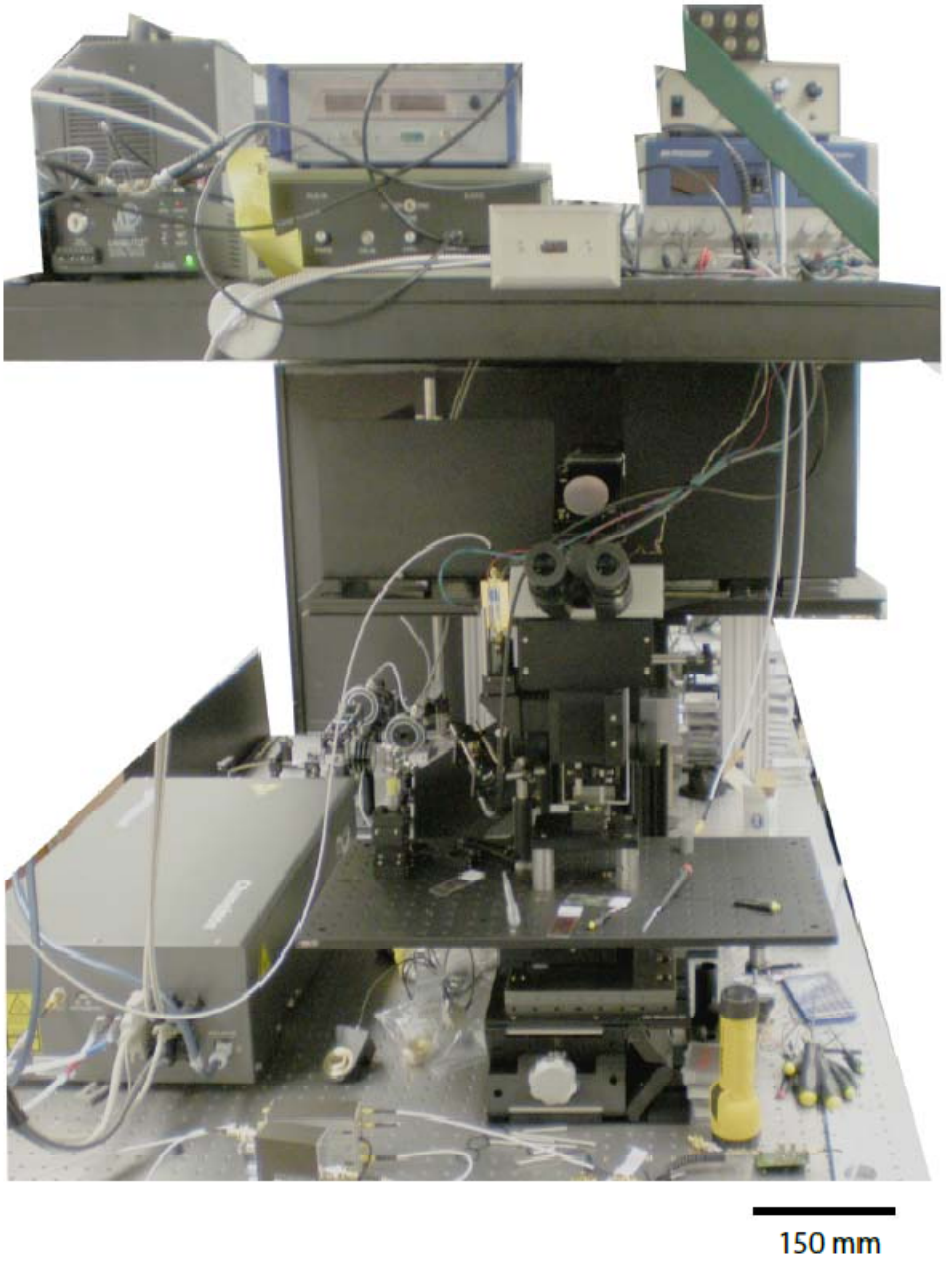

Figure 25

Spatio-temporal multiplexing 2PLSM microscope prototype assembled

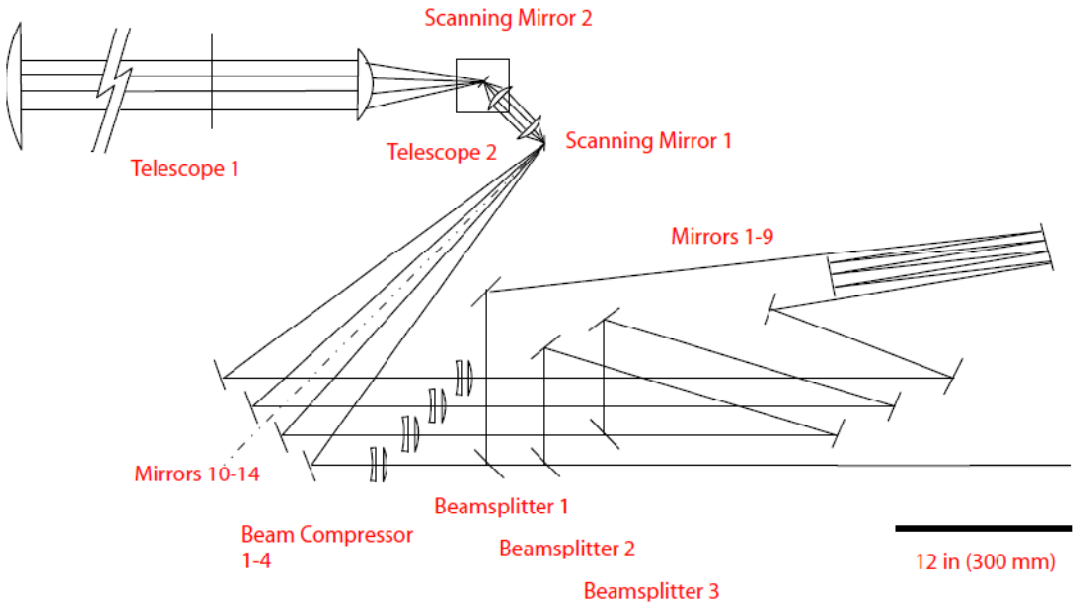

Figure 26

Scale drawing of delay and scanning optical path

Layout of the optical path in the delay line section requires that each beam be delayed by 3 ns. For a prototype, using fewer mirror reflections allows for ease of alignment, as alignment errors compound with increasing reflections. Note that input polarization must be vertical, and an optical plane well defined. Future compact designs including more beams may utilize increased beam folding for reducing cost and space. Galilean beam compressors are added to prepare beam diameters for scanning mirrors. These can be removed in future versions.

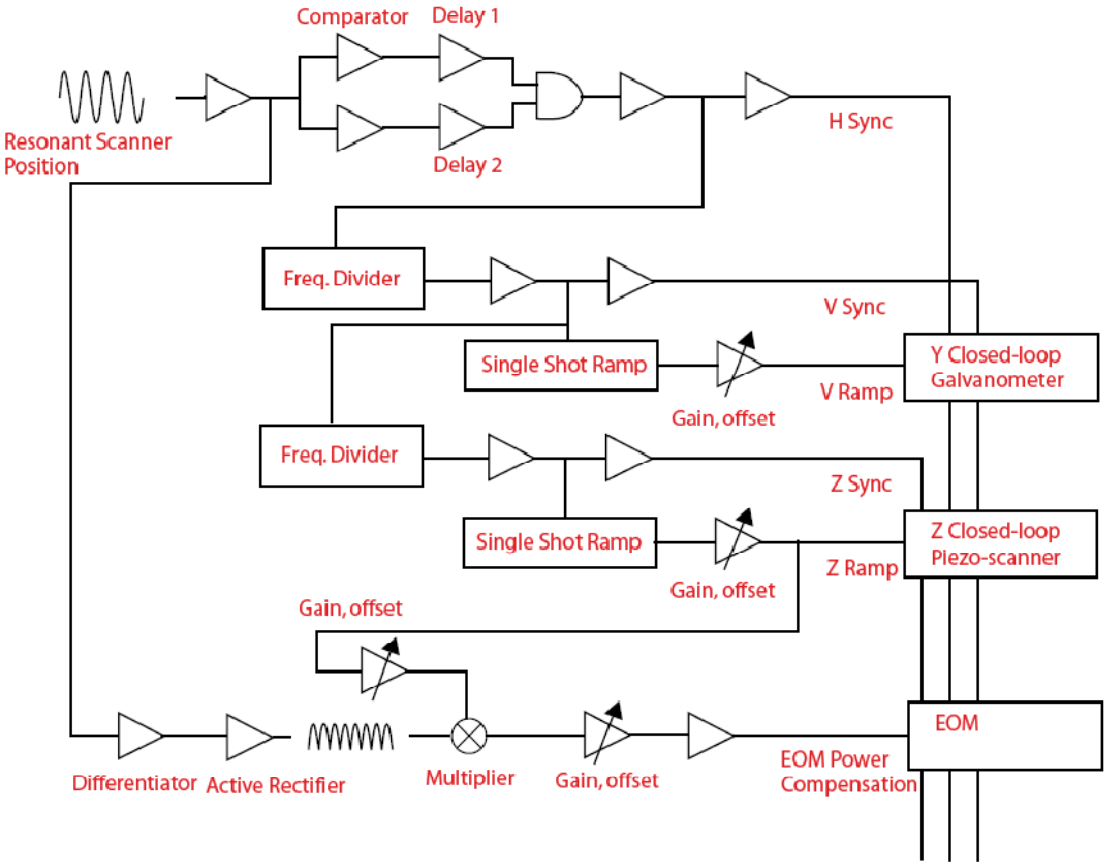

Figure 27

Laser scanning confocal microscope control electronics schematic

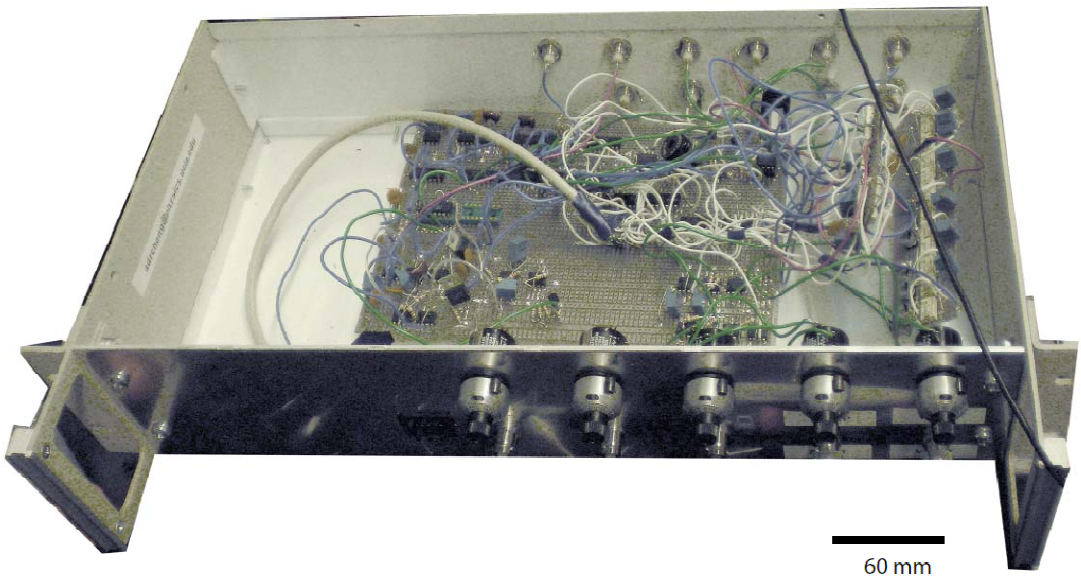

Figure 28

Laser scanning confocal microscope control electronics assembled

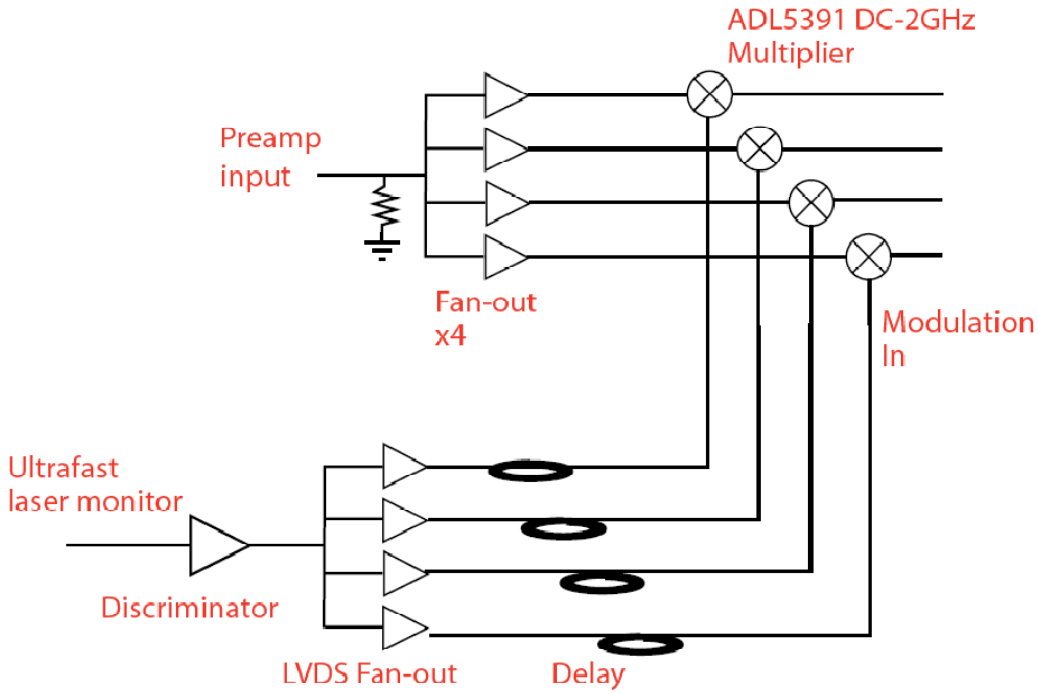

Figure 29

Demodulation electronics schematic

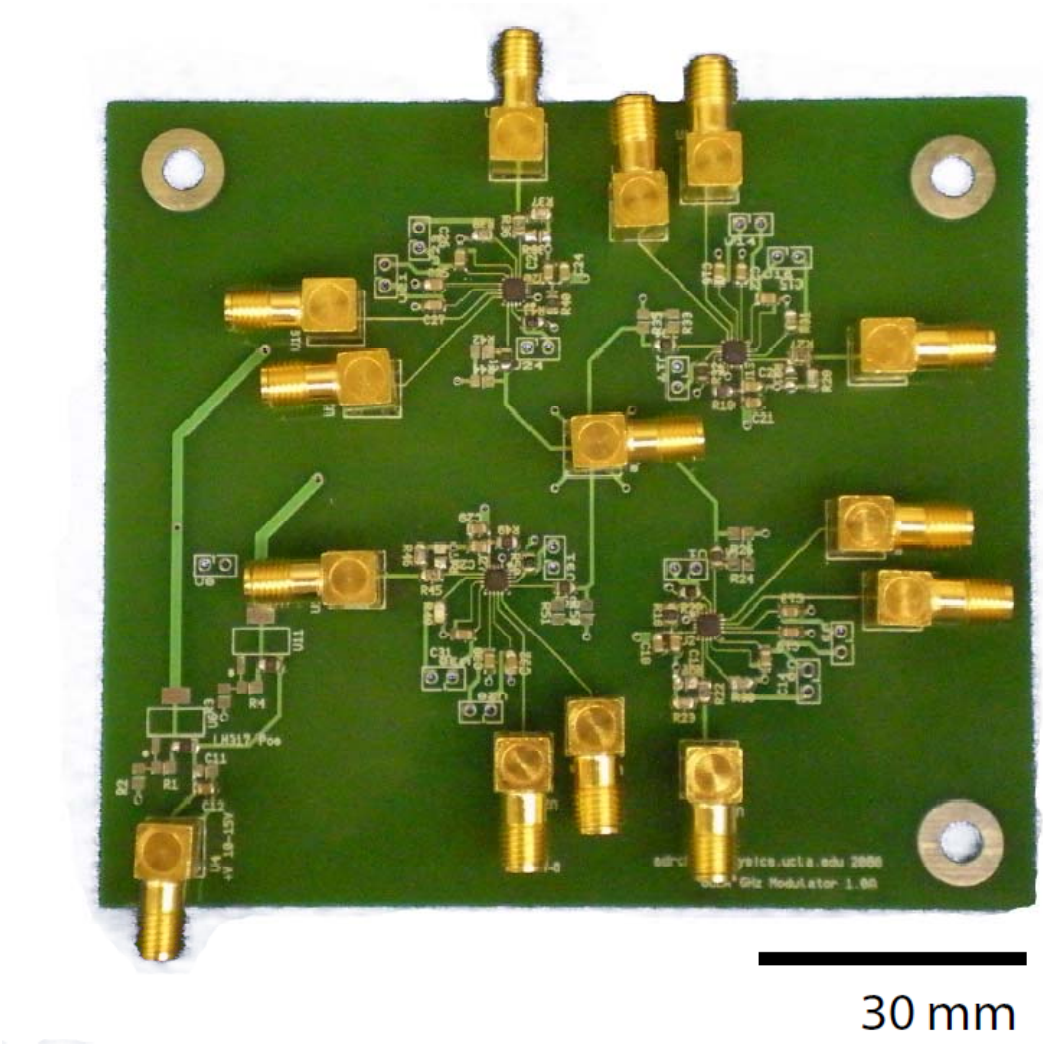

Figure 30

Assembled demodulation electronics circuit board

Table 1

Comparison of laser scanning methods for high-speed deep-tissue MPM and confocal LSM

Method	Highest Rate	Issues	Advantage	Descan
Closed-loop galvanometer	500Hz line rate		Linear control	Yes
Resonant galvanometer	32kHz line rate	Sinusoidal, non-variable rate	100% aperture usage vs polygonal mirror, high rate	Yes
Polygonal mirror (72 faces)	32kHz line rate	Minor vibration, aperture issues at high rate	Linear ramp scan pattern, high rate	Yes
Acousto/Electro-optic Deflector (AOD/EOD)	1us per pixel	Dispersive, multi-order, aperture issues at high rate	Fast random access, 3D scanning possible	No
Piezo steering mirror	500Hz line rate	Poor offerings at high rate, low angular deflection	Linear control	Yes
Digital micromirror device (DMD)	1us per pixel binary change	Low power utility for scanning applications	Arbitrary incoherent intensity pattern	Yes
Liquid Crystal on Silicon Spatial Light Modulator (LCOS SLM)	1-10Hz pattern change	Dispersive	Phase control, arbitrary patterns/field shape	No
Nipkow Disk/Spinning Disk	1kHz frame rate	Low power utility, requires imaging detector, minor vibration	Highest rate	No
Piezo scanning stage	500Hz line rate for small loads	Expensive, load dependent rate	Sub-nanometer closed-loop accuracy/stability	Yes
Deformable mirror	1Hz wavefront change	Slow	Implements adaptive optics (AO)	Yes
Micro-electro mechanical system mirror (MEMS)			For miniature systems	

Table 2

Comparison of photodetectors

Photodetector	QE (500nm)	Gain	Rise time/f	Notes
Bi-alkali PMT	10%	10^4 – 10^7	3 ns	Standard, mature
GaAsP PMT	45%	10^4 – 10^7	3 ns	< 1nA photocathode current
Fast PMT (multichannel)	depends	10^4 – 10^7	0.5 ns	Various structures
MCP-PMT	depends	To 10^5	0.1 ns	< 100nA anode/strip current
HAPD	45%	To 10^5	< 0.5 ns	High multi PE linearity
PIN Photodiode (single channel or array)	90%	1	to 1GHz	Low gain
APD (linear mode)	90%	To 300	To 1GHz	Low first stage gain
APD (Geiger mode/SPAD)	90%	mV level counting	10 MHz Count rate	Only photon counting, small area
CMOS/CCD Sensor	To 90%	10-100e-/bit	To 10KHz (1Mpx)	Ubiquitous
Cooled CCD	To 90%	3e- read noise	10 Hz	Low dark current
EMCCD	To 90%	10^6	100 Hz	Single photon sensitive Low first stage gain
EBCCD	10%	10^3	10-100 Hz	Obsoleted by EMCCD
MPPC	70% eff.	To 10^7	To 1ns	Multiple SPAD Very high multi PE Linearity High dark current
Streak Camera	10%	10^2	1ms phosphor	High time resolution

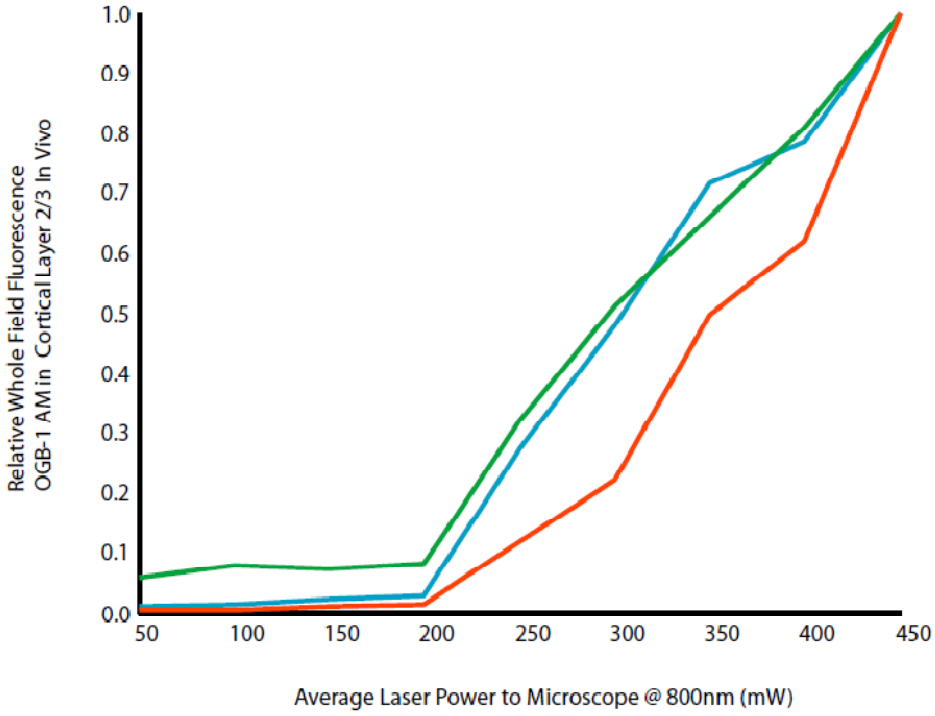

Figure 31

Measured non-linear excitation yield and photon flux limits in 2PLSM

Methods for increasing photon flux need to be explored in order to increase SNR in 2PLSM calcium imaging in-vivo. Shown here is a measurement of in situ signal brightness with increasing excitation power for three preparations. This verifies that signal increases somewhat non-linearly with increasing average excitation power. Both energy per pulse and average power can be increased to yield more fluorescence. Microscope optical efficiencies must be maximized to allow for higher input power, and average power (linear) and pulse energy (non-linear) damage thresholds must be characterized to understand the limitations of power increase.

Table 3

Optical Train Efficiencies

Optical Train Section	Power available at this section in existing 2PLSM system	Power available at this section in 2PLSM prototype
Before microscope	100%	100%
After delays	N.A.	82%
After X-Y scanners	40%	58%
Back aperture	40%	57%
After Olympus 40x 0.8NA water dipping objective	12%	36%
After Zeiss 40x 1.0 NA water dipping objective	15%	41%

In vivo cranial window preparation and calcium dye injection

We used male and female juvenile c57Bl/6 mice (n= 8; postnatal days 15-21) for all experiments. We followed protocols published online by our laboratory [29-30]. A modified cranial window surgery, in which the glass coverslip only partially covers the dura, leaving a gap for injecting the calcium indicator was performed under light isoflurane anesthesia (0.5-1% in O_2). Sulforhodamine (SR) 101 was also injected to label astrocytes. With 2-4 injections of the calcium dye per animal we can label hundreds of Layer 2/3 neurons over a large area (1 mm^2). 2-photon calcium imaging (800 nm) of Fluo-4 AM began after a 30-60 min recovery period. We used 40X 1.0 NA (Zeiss) or 40X 0.8 NA (Olympus) objectives. The emission of SR101 in the red channel (filter 629/53 nm) was separated from that of the calcium dye in a green channel (filter 525/50 nm) with a dichroic that transmits above 562 nm. Calcium imaging was done under isoflurane anesthesia. Several 160 second-long image sequences were recorded, consisting of 40,000 frames (field of view measuring ~250 x 250 µm, 800 x 500 pixels acquired at 250 frame/s.

Electrophysiological recordings

In vivo loose cell-attached recordings were performed as previously described [10], using a patch clamp amplifier (Model 2400, A-M Systems, Sequim, WA) and borosilicate microelectrodes (4-6 MΩ) filled with a potassium gluconate solution containing (in mM) 105 K-gluconate, 30 KCl, 10 HEPES, 10 phosphocreatine, 4 ATP-Mg, 0.3 GTP (adjusted to pH 7.3 with KOH). Cells were targeted using the shadow-patch method [31].

Image processing and data analysis

Image processing was done with custom code written in MATLAB. Images were first transformed using linear interpolation to correct for the sinusoidal resonant scanner trajectory. Contours of cells were detected by a combination of static and dynamic methods. Cells with high baseline calcium indicator fluorescence were detected by taking mutually exclusive regions in the 2 x 2 median filtered stack sum with eccentricity < 0.9, area between 500 and 1200 μm, and perimeter less than twice that of a circle with the same radius. These regions were accumulated over trials with image binarization threshold between 0 and 1 with 50 steps. Cells with low baseline calcium indicator fluorescence but high activity were detected by repeating the process, except with an image representing the integrated frequency of image pixel fluctuation above 2 standard deviations over time after linear drift subtraction and 8 x 8 spatial and 32-fold temporal binning. Once cells were identified, raw calcium imaging traces were calculated with linear drift subtracted. Raw traces were deconvolved with a normalized

1 s exponential kernel using the z-transform rather than an IIR filter (long division) [8]. This allowed a Wiener parameter of 0.05 to be used when dividing the raw trace z-transform by the exponential z-transform, to increase stability. Finally, a finite impulse response low pass filter was run.

Signal-to-noise ratio in 2-photon calcium imaging

A key motivation for the introduction of multiple beams for in vivo 2-photon calcium imaging was to address the critical problem of limited signal-to-noise ratio (SNR) that largely determines the microscope's performance for single action potential detection. With the use of single-photon sensitive detectors, the largest noise component is generally shot noise, giving a SNR proportional to $N^{1/2}$, where N is the number of photons per cell per image frame. In the case where other noise factors are small, this means 10^4-10^6 photons are required per cell per frame to resolve single action potential signals, which usually result in only a few percent change in fluorescence. This makes increasing throughput challenging, when detected signal levels of 1 photoelectron per laser pulse are typical. Due to the non-linear nature of 2-photon excitation, some have had success increasing laser energy per pulse [27], while others have encountered a non-linear photo-damage or saturation limit [28,32]. In this case, increasing the number of laser pulses can overcome this barrier and deliver a greater signal. In principle, deep tissue 2PSLM with multiple beams allows signal level and

scanning rate to be increased proportionally, preserving SNR. In addition, as ultrafast lasers with higher average output power become available, pulse splitting [28] could also be incorporated within each multiplexed beam to further increase brightness. Further studies will be needed to measure the various photo-damage and saturation limits relevant to typical imaging experiments in order to determine the optimal number of beams.

Using our prototype system, with 100 cells filling approximately 30-50% of the field of view, we achieved a shot noise-limited time resolution of approximately 20 Hz (not shown). The neuropil signal comprises the remaining part of the frame and correspondingly contains high time resolution. To eventually achieve useful time resolution equivalent to the frame scanning rate, one could exploit a variety of brightness enhancing techniques, such as collecting scattered light with fiberoptic light guides [33] or excitation wavefront and pulse optimization. Furthermore, while increasing brightness increases SNR by the square root, lowering the read noise via improved read out electronics or photon counting methods, or improvements in calcium indicator signals would go even further, improving SNR proportionally.

Spatio-temporal multiplexing for fluorophores with longer lifetimes

The simplest way to extend spatio-temporal multiplexing to fluorophores with longer lifetimes is to decrease the laser repetition rate while maintaining average laser power (and hence increasing pulse energies), for example using bragg cell laser cavity

modulation or increasing the overall cavity length. This would have the secondary benefit of increasing excitation efficiency. Another possible approach is to use FLIM-based deconvolution of spatio-temporally multiplexed images of longer lifetime fluorophores, but would require very good signal to noise ratio. Finally, decreasing fluorescence decay times might help, for example using spectroscopic pump-probe techniques that stimulate fluorescence emission. In the same way, using voltage-dependent second harmonic generation with certain fluorophores could be advantageous, since the resulting light signal occurs instantly rather than over several nanoseconds.

Combining spatio-temporal multiplexing with AODs and arbitrary line scanning

The spatio-temporal multiplexing technique we describe could be combined with other approaches to increase the speed of 2-photon calcium imaging, including random access point scanning with AODs or arbitrary free line scanning systems (reviewed in Ref. [34]). AODs allow millisecond 3-D time resolution by scanning a limited number of points coinciding with cell bodies [35]. However, the axial extent of scanning with AODs is less than 50 μm and the number of AODs necessary to implement 3-D scanning introduces considerable spatial and temporal dispersion, as well as power loss. The arbitrary targeted path scanning technique takes advantage of closed-loop scanning mirrors to scan optimized contours coinciding with cell bodies [36]; for 3-D imaging, this

approach can be used in combination with a piezo-electric objective scanner, resulting in acquisition rates of several Hz for small volumes [37]. Although neither of these techniques affords full image sampling, and advantage of AODs is that they confine scanning solely to relevant regions (e.g., cell bodies but not the neuropil). By contrast, the raster scanning approach using multiple beams that we used preserves full frame image scanning, which allows a full range of image processing methods for cell identification and image registration to be used, and generally simplifies data interpretation and analysis.

To realize optimally increased throughput using spatio-temporal multiplexing, AOD-based and contour scanning systems require independent beam scanning, rather than the fixed beam pattern used for raster scanning. This requires multiple sets of x-y scanners and simultaneous projection of their apertures on to the objective back aperture. One solution could be to simply project the apertures of multiple sets of AODs or closed-loop scanning mirrors on to the objective back aperture with different access angles. This would allow each individual beam to scan distinct domains. To achieve independent beam scanning in the same domain, polarization optics generally provide a passive solution for combining the optical paths of two sets of scanners, while EOMs could be used with polarizing beam splitters and polarization rotators to dynamically combine many scanners. Availability of more elegant solutions will depend on the specific scan method and pattern.

Beam cross talk

We measured the potential beam cross-talk due to the finite fluorescence lifetime of the dye compared to the 3 ns beam delays during normal experimental imaging conditions. A region of barrel cortex was stained with Fluo-4 AM and in vivo calcium imaging was carried out as in Fig. 3, with different beams scanning different axial planes in 3-D. First, a 45 second time-lapse sequence of images was obtained with only beam 2 scanning the tissue (the other beams were blocked). Next, 1 minute later, another 45 second time-lapse sequence of images was obtained with only beam 1. A final 45 second time-lapse sequence was taken with beams 1 and 2 scanning the tissue at different planes (30 μm apart in the z direction). This last calcium 'movie' is subject to crosstalk between beams. Regions of interest (ROIs) around Fluo-4 labeled cells in the beam 2 image plane were manually selected and their average pixel intensity throughout the movie was calculated. The average "leak-through" (γ) of beam 1 into the beam 2 image was calculated using the following equation,

$$C(x,y) = A(x, y) + \gamma(x,y)\, B(x,y)$$

where A is the pixel intensity in the beam 2 alone image, B is the pixel intensity in the beam 1 alone image, and C the pixel intensity in the beam 2 image when simultaneously scanning with beam 1. Cross talk varied for different ROIs presumably because the

lifetime of Fluo-4 changes with [Ca^{2+}], but the average leak-through was 3.0 ± 4.1% (mean ± st. dev.). Cross-talk probably also varies slightly both spatially due to other fluorophore compositions (e.g., autofluorescence), and also temporally (e.g., neuronal activity), which is why these measurements were done over 45 sec. For example, if cross-talk occurs during a 10% ΔF/F leak-through calcium transient, the contribution of this transient to the adjacent beam would be small (~0.3%). This effect will be around the same order as shot noise in our system. This effect will be even in smaller in practice because the fluorescence lifetime of Fluo-4 decreases during a calcium transient.

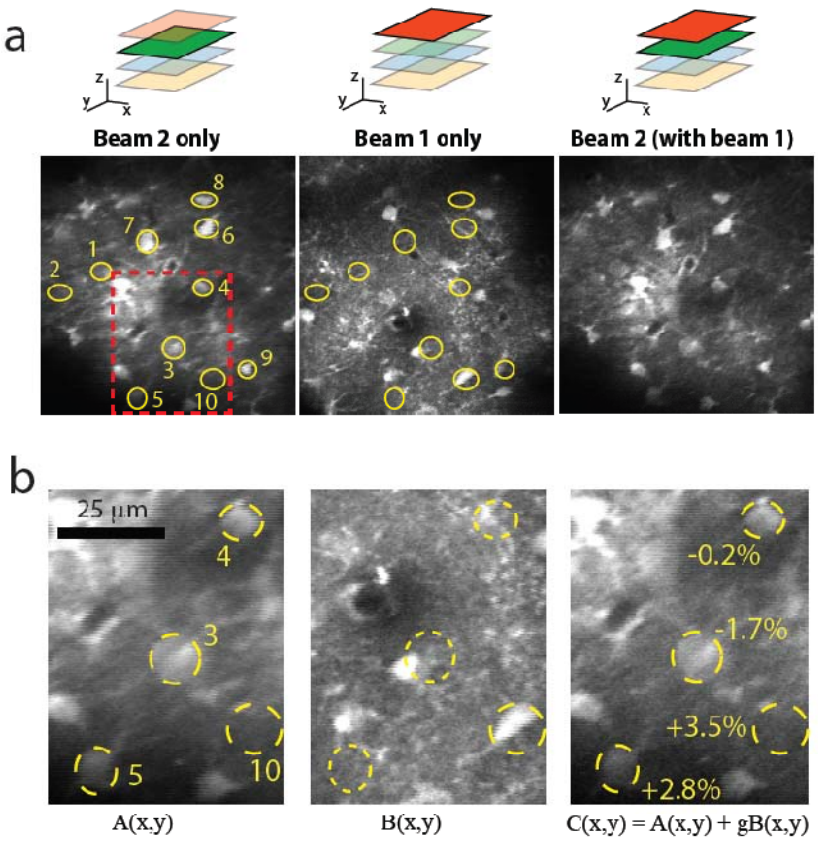

Figure 32

Cross-talk measurement during in-vivo imaging due to finite fluorescence lifetime

(a) Field of view scanned with beam 2 alone (left), beam 1 alone (middle), keeping other beams blocked, and field of view of beam 2 while simultaneously scanning with beam 1 (right). These images were acquired using the 3-D spatiotemporal multiplexing configuration and are average intensity xyt projections of 45 sec-long in vivo calcium imaging movies. Regions of interest (yellow outlines) were selected around somas of presumed neurons (ROIs 1-9) and neuropil (ROI 10) in the beam 2 image. Note that bright astrocytes seen in layer 1 (beam 1 image) are not present in the beam 2 image. The rectangular region outlined in the left panel (red box) is shown at higher zoom in *b*. (b) Higher magnification detail of boxed region in panel *a*. Examples of cross talk values are shown for 3 representative cell body ROIs and 1 neuropil ROI. The average intensity change in beam 2 ROIs in the presence of beam 1 excitation was 3.0 ± 4.1 % (mean ± st. dev.), suggesting that fluorescence leak-through between beams is not a dominant noise factor (see Methods).

References

1 Denk, W., Strickler, J. H. & Webb, W. W. Two-photon laser scanning fluorescence microscopy. *Science* **248**, 73-76 (1990).

2 Svoboda, K., Denk, W., Kleinfeld, D. & Tank, D. W. In vivo dendritic calcium dynamics in neocortical pyramidal neurons. *Nature* **385**, 161-165, doi:10.1038/385161a0 (1997).

3 Loew, L. M. Design and characterization of electrochromic membrane probes. *J Biochem Biophys Methods* **6**, 243-260 (1982).

4 Kao, J. P., Harootunian, A. T. & Tsien, R. Y. Photochemically generated cytosolic calcium pulses and their detection by fluo-3. *J Biol Chem* **264**, 8179-8184 (1989).

5 Poenie, M. & Tsien, R. Fura-2: a powerful new tool for measuring and imaging [Ca2+]i in single cells. *Prog Clin Biol Res* **210**, 53-56 (1986).

6 Palmer, A. E. & Tsien, R. Y. Measuring calcium signaling using genetically targetable fluorescent indicators. *Nat Protoc* **1**, 1057-1065, doi:nprot.2006.172 [pii]
10.1038/nprot.2006.172 (2006).

7 Grewe, B. F. & Helmchen, F. Optical probing of neuronal ensemble activity. *Curr Opin Neurobiol* **19**, 520-529, doi:S0959-4388(09)00125-1 [pii]
10.1016/j.conb.2009.09.003 (2009).

8 Yaksi, E. & Friedrich, R. W. Reconstruction of firing rate changes across neuronal populations by temporally deconvolved Ca2+ imaging. *Nat Methods* **3**, 377-383, doi:nmeth874 [pii]
10.1038/nmeth874 (2006).

9 Born, M. & Wolf, E. *Principles of optics; electromagnetic theory of propagation, interference, and diffraction of light*. (Pergamon Press, 1959).

10 Golshani, P. G., JT; Khoshkhoo, S; Mostany, R; Smirnakis, S; Portera-Cailliau, C. Internally mediated developmental desynchronization of neocortical network activity. *J Neurosci* **in press** (2009).

11 Kerr, J. N. *et al.* Spatial organization of neuronal population responses in layer 2/3 of rat barrel cortex. *J Neurosci* **27**, 13316-13328, doi:27/48/13316 [pii]
10.1523/JNEUROSCI.2210-07.2007 (2007).

12 Sato, T. R., Gray, N. W., Mainen, Z. F. & Svoboda, K. The Functional Microarchitecture of the Mouse Barrel Cortex. *PLoS Biol* **5**, e189, doi:06-PLBI-RA-2351 [pii]
10.1371/journal.pbio.0050189 (2007).

13 Bewersdorf, J., Pick, R. & Hell, S. W. Multifocal multiphoton microscopy. *Opt Lett* **23**, 655-657, doi:36702 [pii] (1998).

14 Nielsen, T., Fricke, M., Hellweg, D. & Andresen, P. High efficiency beam splitter for multifocal multiphoton microscopy. *J Microsc* **201**, 368-376, doi:jmi852 [pii] (2001).

15 Ichihara A, Tanaami T, Isozaki K & Y, S. High-speed confocal fluorescence microscopy using a Nipkow scanner with microlenses for 3D-imaging of single fluorescent molecule in real time. *Bioimages* **4**, 57 (1996).

16 Svoboda, K. & Yasuda, R. Principles of two-photon excitation microscopy and its applications to neuroscience. *Neuron* **50**, 823-839 (2006).

17 Helmchen, F. & Denk, W. Deep tissue two-photon microscopy. *Nat Methods* **2**, 932-940, doi:nmeth818 [pii]
10.1038/nmeth818 (2005).

18 Oheim, M., Beaurepaire, E., Chaigneau, E., Mertz, J. & Charpak, S. Two-photon microscopy in brain tissue: parameters influencing the imaging depth. *J Neurosci Methods* **111**, 29-37 (2001).

19 Niesner, R., Andresen, V., Neumann, J., Spiecker, H. & Gunzer, M. The power of single and multibeam two-photon microscopy for high-resolution and high-speed deep tissue and intravital imaging. *Biophys J* **93**, 2519-2529, doi:S0006-3495(07)71506-0 [pii]
10.1529/biophysj.106.102459 (2007).

20 Crepel, V. *et al.* A parturition-associated nonsynaptic coherent activity pattern in the developing hippocampus. *Neuron* **54**, 105-120, doi:S0896-6273(07)00203-6 [pii]
10.1016/j.neuron.2007.03.007 (2007).

21 Sanderson, M. J. & Parker, I. Video-rate confocal microscopy. *Methods Enzymol* **360**, 447-481 (2003).

22 Fan, G. Y. *et al.* Video-rate scanning two-photon excitation fluorescence microscopy and ratio imaging with cameleons. *Biophys J* **76**, 2412-2420 (1999).

23 Michalet, X. *et al.* Hybrid photodetector for single-molecule spectroscopy and microscopy. *Proceedings of SPIE* **6862**, 0F1-0F12 (2008).

24 Greenberg, D. S., Houweling, A. R. & Kerr, J. N. Population imaging of ongoing neuronal activity in the visual cortex of awake rats. *Nat Neurosci* **11**, 749-751, doi:nn.2140 [pii]
10.1038/nn.2140 (2008).

25 Amir, W. *et al.* Simultaneous imaging of multiple focal planes using a two-photon scanning microscope. *Opt Lett* **32**, 1731-1733, doi:138230 [pii] (2007).

26 Yoshiki, K., Azuma, H., Yoshioka, K., Hashimoto, M. & Araki, T. Finding optimal calcium ion probes for fluorescent lifetime measurement. *Optical Review* **12**, 415-419 (2005).

27 Theer, P., Hasan, M. T. & Denk, W. Two-photon imaging to a depth of 1000 microm in living brains by use of a Ti:Al2O3 regenerative amplifier. *Opt Lett* **28**, 1022-1024 (2003).

28 Ji, N., Magee, J. C. & Betzig, E. High-speed, low-photodamage nonlinear imaging using passive pulse splitters. *Nat Methods* **5**, 197-202, doi:nmeth.1175 [pii] 10.1038/nmeth.1175 (2008).

29 Mostany, R. & Portera-Cailliau, C. A craniotomy surgery procedure for chronic brain imaging. *J Vis Exp*, doi:680 [pii] 10.3791/680 (2008).

30 Golshani, P. & Portera-Cailliau, C. In vivo 2-photon calcium imaging in layer 2/3 of mice. *J Vis Exp*, doi:681 [pii] 10.3791/681 (2008).

31 Kitamura, K., Judkewitz, B., Kano, M., Denk, W. & Hausser, M. Targeted patch-clamp recordings and single-cell electroporation of unlabeled neurons in vivo. *Nat Methods* **5**, 61-67, doi:nmeth1150 [pii] 10.1038/nmeth1150 (2008).

32 Hopt, A. & Neher, E. Highly nonlinear photodamage in two-photon fluorescence microscopy. *Biophys J* **80**, 2029-2036, doi:S0006-3495(01)76173-5 [pii]

10.1016/S0006-3495(01)76173-5 (2001).

33 Engelbrecht, C. J., Gobel, W. & Helmchen, F. Enhanced fluorescence signal in nonlinear microscopy through supplementary fiber-optic light collection. *Opt Express* **17**, 6421-6435, doi:178935 [pii] (2009).

34 Wilt, B. A. *et al.* Advances in light microscopy for neuroscience. *Annu Rev Neurosci* **32**, 435-506, doi:10.1146/annurev.neuro.051508.135540 (2009).

35 Duemani Reddy, G., Kelleher, K., Fink, R. & Saggau, P. Three-dimensional random access multiphoton microscopy for functional imaging of neuronal activity. *Nat Neurosci* **11**, 713-720 (2008).

36 Lillis, K. P., Eng, A., White, J. A. & Mertz, J. Two-photon imaging of spatially extended neuronal network dynamics with high temporal resolution. *J Neurosci Methods* **172**, 178-184, doi:S0165-0270(08)00252-5 [pii] 10.1016/j.jneumeth.2008.04.024 (2008).

37 Gobel, W., Kampa, B. M. & Helmchen, F. Imaging cellular network dynamics in three dimensions using fast 3D laser scanning. *Nat Methods* **4**, 73-79 (2007).